NASA Contractor Report - 177343-VOL-4

[redacted]

Propulsion and Airframe Aerodynamic Interactions of Supersonic V/STOL Configurations

Volume IV: Final Report - Summary

D.E. Zilz
H.W. Wallace
P.E. Hiley

CONTRACT NAS2-10791
SEPTEMBER 1985

NASA

NASA Contractor Report - 177343

Propulsion and Airframe Aerodynamic Interactions of Supersonic V/STOL Configurations

Volume IV: Final Report - Summary

D.E. Zilz
H.W. Wallace
P.E. Hiley
McDonnell Aircraft Company
St. Louis, Missouri

Prepared for
Ames Research Center
Under Contract NAS2-10791
September 1985

National Aeronautics and
Space Administration

Ames Research Center
Moffett Field, California 94035

FOREWORD

This report was prepared by McDonnell Aircraft Company (MCAIR), a component of McDonnell Douglas Corporation, St. Louis, Missouri, for the National Aeronautics and Space Administration, Ames Research Center. The study was performed under NASA Contract NAS2-10791, "Propulsion and Airframe Aerodynamic Interactions of Supersonic V/STOL Configurations". The work was performed from October 1980 through September 1985 with R. O. Bailey as the NASA ARC Technical Representative. The program was accomplished under the direction of P. E. Hiley, Program Manager and H. W. Wallace, Technical Study Manager.

Acknowledgement is also given to S. C. Smith and J. B. Gustie of NASA ARC for their efforts during the calibrations, wind tunnel tests, and data analysis at the NASA ARC Unitary Plan 11-Foot Transonic Wind Tunnel.

This report was prepared by P. E. Hiley, H. W. Wallace, and D. E. Zilz of MCAIR. The authors are indebted to the following MCAIR personnel for their assistance during the study: M. R. Mraz, P. A. Devereaux, A. V. Arena, and M. E. Booher of Propulsion and Thermodynamics.

The authors also commend J. C. Poole, W. Cerski, and C. C. Smithson of the MCAIR Aerodynamics and Propulsion Laboratories for their efforts in the design and testing of the wind tunnel models.

Special acknowledgements are also due K. H. Token and D. W. Esker of MCAIR (Propulsion and Thermodynamics), who, in their supervisory positions, have made valuable contributions to the program and this report.

This report was submitted in four volumes by the authors in September 1985.

TABLE OF CONTENTS

LIST OF ILLUSTRATIONS

LIST OF ILLUSTRATIONS

LIST OF ILLUSTRATIONS (Continued)

LIST OF ABBREVIATIONS AND SYMBOLS

Symbol	Definition
A/B	Afterburning power setting on nozzle
A_c	Inlet capture area ($35.23cm^2$)
AF	Axial Force
A_o	Total inlet captured stream tube area (cm^2)
ALBEN	Aerodynamically Load Balanced Exhaust Nozzle
ALPHA, AOA	Model angle of attack (Deg)
A_{TH}	Nozzle throat area
b_c	Model canard span (52.49cm)
b_w	Model wing span (130.30cm)
B.L.	Model butt line
$\bar{c}_c$	Mean aerodynamic canard chord (19.60cm)
C_D	Total aircraft drag coefficient ($C_{D_A} + C_{D_{NOZ}}$)
C_{D_A}	Metric airframe drag coefficient
$C_{D_{NOZ}}$	Exhaust nozzle drag coefficient (2 nozzles)
C_L	Total aircraft lift coefficient ($C_{L_A} + C_{L_{NOZ}}$)
C_{L_A}	Metric airframe lift coefficient
$C_{L_{NOZ}}$	Exhaust nozzle lift coefficient (2 nozzles)
C_M	Total aircraft pitching moment coefficient
C_{M_o}	Total aircraft pitching moment coefficient at zero lift
C_{M_A}	Metric airframe pitching moment coefficient
CMCRB	Canard root bending moment coefficient ($MCRB/(S_c b_s Q)$)
$\bar{c}_w$	Mean aerodynamic wing chord (41.70cm)
C_p	Pressure coefficient $[(P_L-P_o)/Q_o]$
CMAPS	Compact Multimission Aircraft Propulsion Simulator
DDA	Detroit Diesel Allison
DLE	Direct Lift Engine
DLI	Deck Launched Intercept (mission)
DPDS	Static pressure differential across inlet duct seal
Dry	Dry power setting on nozzle

LIST OF ABBREVIATIONS AND SYMBOLS (CONTINUED)

Symbol	Definition
ES	Engine station
F/T, FT	Flow-Through test mode
FS	Fuselage Station
J/E, JE	Jet-Effects test mode
L/C	Lift/Cruise
Mach, M	Free stream Mach number
MCAIR	McDonnell Aircraft Company
MCRB	Canard root bending moment
MFR, MFRA	Average of left and right Inlet Mass Flow Ratios based on calibration correlated to CMAPS turbine exit pressure for Simulator Mode or at nozzle exit chokes for Flow-Through Mode, [A_O/Ac]
MS	Model Station
N	CMAPS Rotor speed (RPM)
NPR, NPRA	Average of left and right Nozzle Pressure Ratios [P_{T_J}/Po]
NRP	Percent of sea-level referenced design rotor speed, ((N/75185) x θ x 100)
P, Po	Free Stream static pressure
P_{base}	Static Pressure at Base of Exit Chokes
P2	Average static pressure at compressor face
P_L	Local Static Pressure
Plane 2	Compressor face
Plane 4	Turbine inlet
Plane 8	Exhaust Nozzle Duct
Plane 15	Compressor discharge
Plane 57	Turbine discharge
PS57	Turbine discharge static pressure
P_T, P_{T_o}	Free stream total pressure
P_{T_2}	Average total pressure at compressor face, left or right
P_{T_8}	Average total pressure at exhaust nozzle

LIST OF ABBREVIATIONS AND SYMBOLS (CONTINUED)

Symbol	Definition
$P_{T_{max}}$	Maximum value of total pressure of compressor face
$P_{T_{min}}$	Minimum value of total pressure at compressor face
P_{T_J}	Total pressure of jet exhaust at nozzle exit
$P_{T_{throat}}$	Average Total Pressure at Nozzle Throat
Q, Qo	Free stream dynamic pressure
RALS	Remote Augmented Lift System
RCS	Reaction Control Systems
SIM	Simulator test mode
SLS	Sea-Level Static
STO	Short Takeoff
t/c	Wing thickness to chord ratio
T_{T_2}	Total Temperature at Plane 2
T_{T_8}	Total Temperature at Plane 8
VCE	Variable Cycle Engines
V/STOL	Vertical/Short Takeoff and Landing
VTO	Vertical Takeoff
VTOL	Vertical Takeoff and landing
W2	Inlet Mass Flow Rate
W8	Nozzle Mass Flow Rate
W2R	Corrected Inlet Airflow $(\frac{W2 * \theta}{\delta})$
$W2R_2$	Corrected Inlet Mass Flow Rate Based on Plane 2 method
$W2R_{15}$	Corrected Inlet Mass Flow Rate Based on Plane 15 method
$W2R_8$	Corrected Inlet Mass Flow Rate Based on Plane 8 method
$W2R_{57}$	Corrected Inlet Mass Flow Rate Based on Plane 57 method
WL	Model water line
WTAP	Mass Flow function $(WB\sqrt{TT8}/(PTB*A_{TH})$
α	ALPHA, Angle-of-Attack (Deg)
θ	Sea-level standard day temperature correction $\sqrt{((T_{T_2} + 460/518.67)}$

Symbol	Definition
θ	Sea-level standard day pressure correction $(\frac{P_{T2}}{14.697})$
δ_c	DELCR or DELCL
δ_f	Wing flap deflection angle, positive trailing edge down (Deg)
δ_n	Nozzle thrust vectoring angle, positive trailing edge down (Deg)
Λ	Wing Sweep Angle (Deg)

SUMMARY

A wind tunnel model of a supersonic V/STOL fighter configuration has been tested to measure the aerodynamic interaction effects which can result from geometrically close-coupled propulsion system/airframe components. The approach was to configure the model to represent two different test techniques. One was a conventional test technique composed of two test modes. In the Flow-Through mode, absolute configuration aerodynamics were measured, including inlet/airframe interactions. In the Jet-Effects mode, incremental nozzle/airframe interactions were measured. The other test technique was a propulsion simulator approach, where a sub-scale, externally powered engine is mounted in the model. This allowed proper measurement of inlet/ airframe and nozzle/airframe interactions simultaneously.

Comparison of the measured aerodynamic characteristics between the two test techniques is a direct indication of the extent to which inlet and nozzle flowfields are coupled together. If significant coupling were to exist, there would be disagreement between the two data sets. The simulator test technique may then be required in the future to properly measure the aerodynamic characteristics of compact fighter configurations.

Measurement of these propulsion/airframe interaction effects was carried out in a three phase experimental program, sponsored by the NASA-Ames Research Center. Conceptual model design was accomplished in Phase 1, detailed model design and fabrication in Phase 2, and high speed testing in Phase 3.

The aerodynamic configuration tested was a canard/wing concept designed for high transonic maneuverability, employing non-axisymmetric, vectorable exhaust nozzles located near the wing trailing edge.

The overall character of the aerodynamic flowfield, including the interactions due to inlet/nozzle coupling, were quantified by comparing force balance data between the different test modes, and by comparing static pressure distributions over the entire model surface.

The data analysis indicated that:

- The net effect of flowfield interactions was relatively small for the tested configuration, which had unvectored nozzles in the afterburning (A/B) power setting.

- The largest effect of inlet/nozzle coupling occurred supersonically, when the simulator technique demonstrated less drag than the conventional technique. Most of the interaction effects were felt on the nozzle external surfaces.

- Inlet MFR variations and canard angle deflections combined to affect nozzle drag in the transonic regime. Inlet fairing effects also propagated the entire length of the nacelle to affect nozzle drag at these speeds.

- The operation of the simulators in a wind tunnel environment was generally reliable, although specific areas will require further development.

1. INTRODUCTION

Configurations proposed for advanced, high speed V/STOL aircraft can have vectoring nozzles, close-coupled inlet/nozzle arrangements, and variable-incidence canards located near the inlets. The complex propulsion/aerodynamic flowfield interactions which may result from these highly integrated designs are illustrated in Figure 1-1. These interactions are difficult if not impossible to evaluate with conventional wind tunnel test techniques. The conventional techniques, using jet-effects and flow-through models, cannot simulate inlet and nozzle flowfields simultaneously, as illustrated in Figure 1-2.

An alternate test technique has been developed which provides simultaneous simulation of inlet and nozzle flowfields by using a Compact Multimission Aircraft Propulsion Simulator (CMAPS). The CMAPS, Figure 1-3, is a miniature jet engine powered by a high pressure air turbine. It can be installed and operated in a sub-scale, supersonic wind tunnel model. A matrix of inlet mass flows and nozzle pressure ratios representative of the full-scale propulsion system can be simulated on a single model.

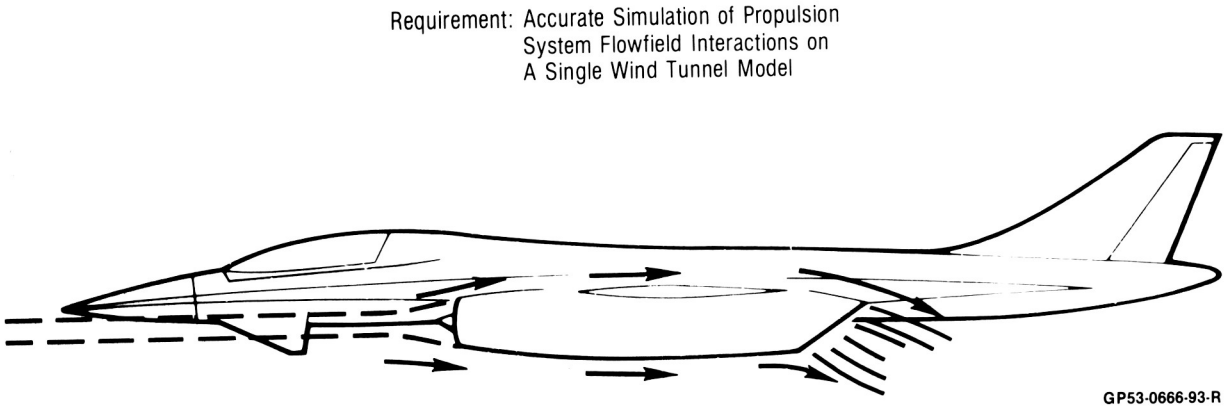

Figure 1-1. Typical Propulsion System Installation Susceptible to Inlet/Nozzle Flowfield Coupling

Jet-Effets Test Technique

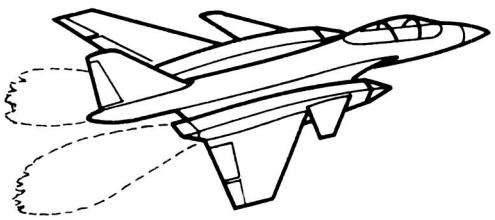

— Proper Aft-End Geometry
— Proper Nozzle Pressure Ratio Simulation

— Improper Inlet Geometry (Inlets Faired)
— No Inlet Flow Simulation

Flow-Through Test Technique

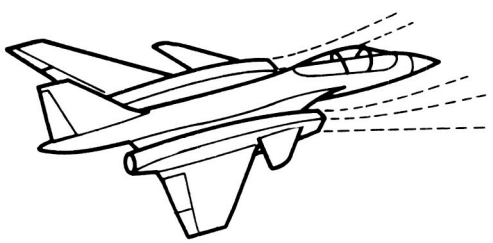

— Distorted Aft-End Geometry
— Improper Nozzle Pressure Ratio Simulation

— Proper Inlet/ Airframe Geometry
— Proper Inlet Mass Flow Ratio Simulation

GP53-0666-92-R

Figure 1-2. Characteristics of Conventional Wind Tunnel Test Techniques

CMAPS Characteristics

Length:	26.4 cm (10.4 in.)
Maximum Diameter:	10.7 cm (4.2 in.)
Compressor Face Diameter	7.6 cm (3.0 in.)
Weight:	5.4 kg (11.8 lb)
Maximum Corrected Airflow:	0.758 kg/sec (1.67 lbm/sec)
Maximum Physical Rotor Speed	88,000 RPM

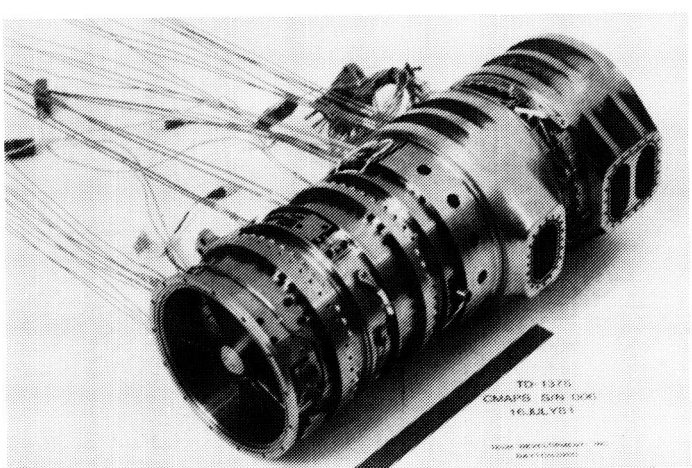

GP53-0666-53-R

Figure 1-3. Compact Multimission Aircraft Propulsion Simulator (CMAPS)

The CMAPS was developed under the auspices of the Air Force Aero Propulsion Laboratory by McDonnell Aircraft Company (MCAIR), General Electric (GE), and Tech Development, Inc., Reference 1.

The NASA-Ames Research Center (ARC) and MCAIR have recently completed an experimental program to evaluate the technology of CMAPS testing in wind tunnel models. This program included design, fabrication, and testing of a supersonic V/STOL fighter model which could accept two propulsion simulators. A photograph of the wind tunnel model with the CMAPS installed is shown in Figure 1-4. This program represented the first time that twin CMAPS were tested in a scale model of a full aircraft configuration. Prior to this program, only single simulators had been tested, and only in a simple nacelle/body wind tunnel model, as described in Reference 2.

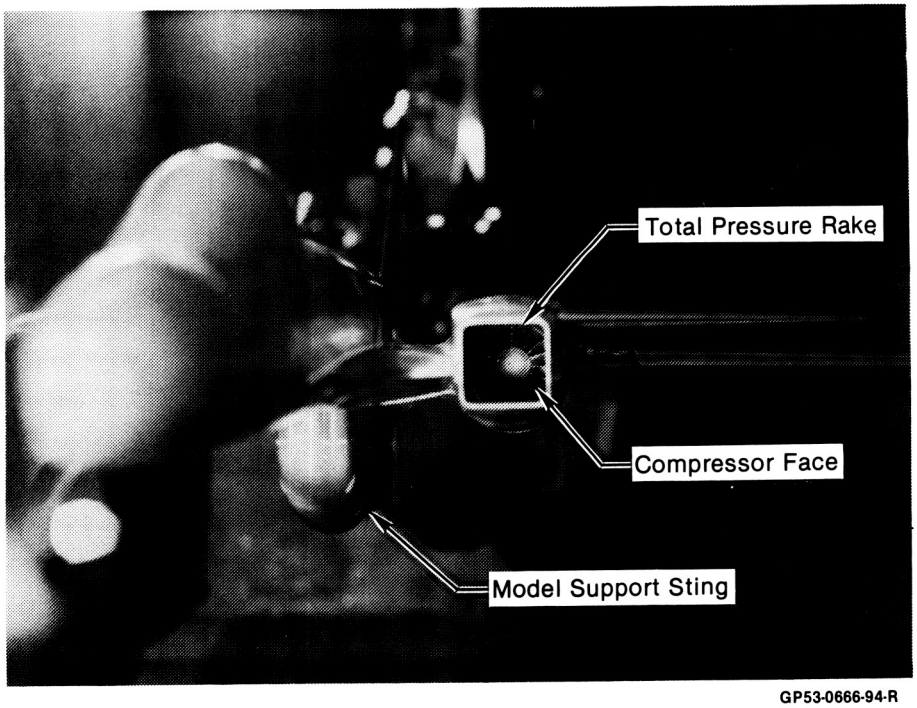

Figure 1-4. Propulsion Simulator Installation

The primary objective of this program was to identify and measure the net effect of inlet-to-nozzle flowfield interactions by using the CMAPS. A secondary objective was to develop the installation and test techniques for CMAPS-equipped wind tunnel models of full aircraft configurations.

The approach was to use both simulator and conventional techniques to test a sub-scale wind-tunnel model of a supersonic V/STOL aircraft which employed a close-coupled propulsion system/airframe arrangement. Any difference identified between the conventional and simulator mode results is an indication of inlet/nozzle flowfield coupling. The model, installed in the NASA-ARC 11 ft transonic wind tunnel, is shown in Figure 1-5. This close-coupled model was originally developed for jeteffects and flow-through testing in the Advanced Nozzle Concepts (ANC) program by the Air Force Wright Aeronautical Laboratories (AFWAL), Reference 3. Under the NASA-ARC program discussed herein, model hardware was designed and fabricated to provide for testing with the propulsion simulators, as well as with jet-effects and flow-through techniques.

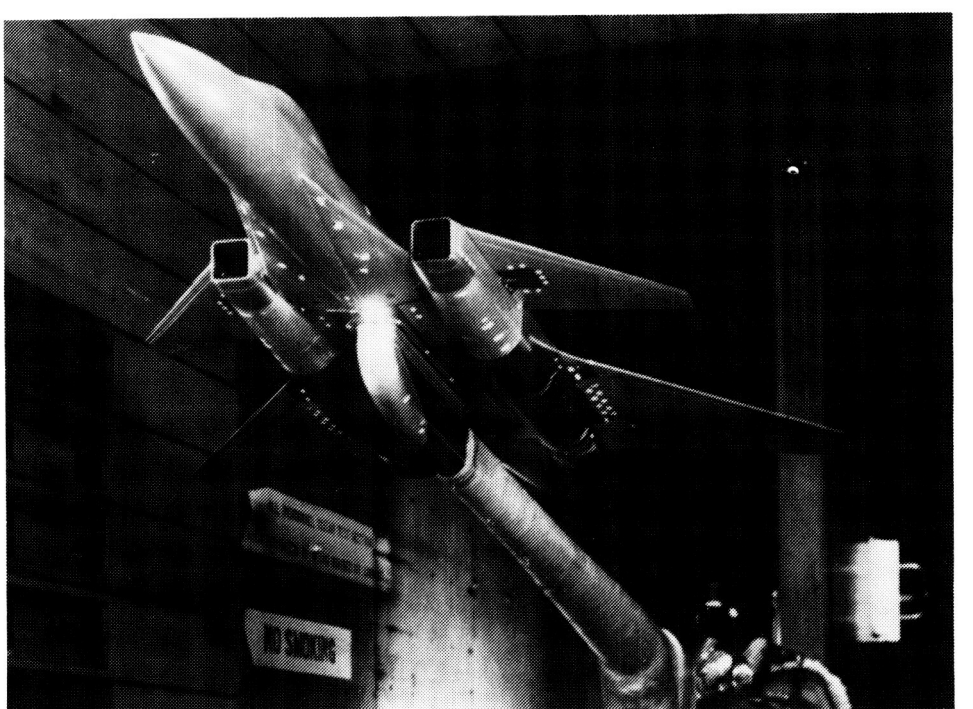

GP53-0666-68-R

Figure 1-5. Supersonic V/STOL Wind Tunnel Model Installed in NASA-Ames Eleven Foot Transonic Wind Tunnel

The results of the wind tunnel tests are presented in a series of three NASA Contractor Reports. The surface pressure data is reported in Volume I (Reference 4), the force and moment data and data reduction procedures in Volume II (Reference 5), and the aerodynamic data analysis in Volume III (Reference 6).

The key program results are summarized in this Final Report, Volume IV. The study configuration is described, and key aerodynamic test results presented. A major section is devoted to the operational experience gained from model design and testing of the CMAPS units in a full configuration wind tunnel model. Recommended improvements are also included.

2. AERODYNAMIC CONFIGURATION DESCRIPTION

An advanced V/STOL aircraft with supersonic fighter/attack capability was selected as the baseline aerodynamic configuration for this study. Considerations in the development of the configuration included the following:

(1) Twin engine propulsion system with vectorable, non-axisymmetric exhaust nozzles.

(2) Propulsion system integration and canard/wing configuration which maximize the aerodynamic effects induced by thrust vectoring.

(3) Configurations with high probability of demonstrating inlet/nozzle flowfield coupling.

(4) Engine cycle compatibility with the CMAPS.

(5) Configurations common to other programs to minimize model fabrication costs.

2.1 FULL SCALE VEHICLE

The full scale vehicle designed in this program was based on a lift plus lift/cruise propulsion system. The configuration is characterized by podded nacelles, inlet mounted canards, and vectorable non-axisymmetric nozzles at the wing trailing edge. The characteristics of the full scale study vehicle are shown in Figure 2-1. In the VTOL mode, forward mounted direct lift engines and vectored Augmented Deflector Exhaust Nozzles (ADENs) on the turbofan lift/cruise engines provided the required normal component of thrust.

A detailed discussion of sizing, selection criteria, and utilization of this V/STOL concept is provided in Volume III (Reference 6).

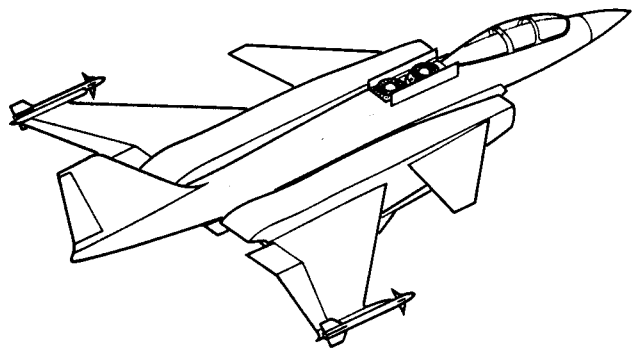

	Propulsion
Engines	(2) Advanced Mixed Flow Turbofans
	(2) Advanced Direct Lift Engines
L/C FNSLSI (ea)	87,314 N (19,630 lb)
DLE FNSLSI (ea)	47,149 N (10,600 lb) - 32°C (90°F) Day
Nozzles	L/C: ADEN-DLE: Eye Lid
Inlet	Normal Shock, $A_C = 0.39$ m^2/Engine (4.2 ft^2/Engine)

GP53-0666-89-R

Figure 2-1. Full Scale Characteristics of Supersonic V/STOL Study Configuration

2.2 SIMULATED V/STOL TEST CONFIGURATION

The scale of a CMAPS-equipped wind tunnel model of this V/STOL configuration is set by matching the maximum airflow of the CMAPS (0.748 kg/sec (1.65 lbm/sec)) to the maximum engine airflow (normally at sea level static condition). Specifically, the model scale factor is determined as follows:

$$\text{Scale Factor} = \sqrt{\frac{\text{Max CMAPS Compressor Corrected Airflow}}{\text{Max Engine Corrected Airflow}}}$$

Application of this relationship to the turbofan engines of the lift/cruise concept (80.7 Kg/sec (178 lbm/sec)) results in a model scale of 9.62%.

An existing wind tunnel model of a similar aerodynamic configuration was made available to this program by the Air Force Wright Aeronautical Laboratories (AFWAL), thus reducing program costs. The basic configuration, shown in Figure 2-2, was developed under prime contract (F33615-77-C-3094) to AFWAL by MCAIR in the Advanced Nozzle Concepts (ANC) program, Reference 3. It is also characterized by widely spaced, podded nacelles, canards and twin vectorable non-axisymmetric nozzles at the wing trailing edge. The nozzle concept is a General Electric Aerodynamic Load Balanced Exhaust Nozzle (ALBEN), with fully continuous vectoring capability to $\pm 30°$.

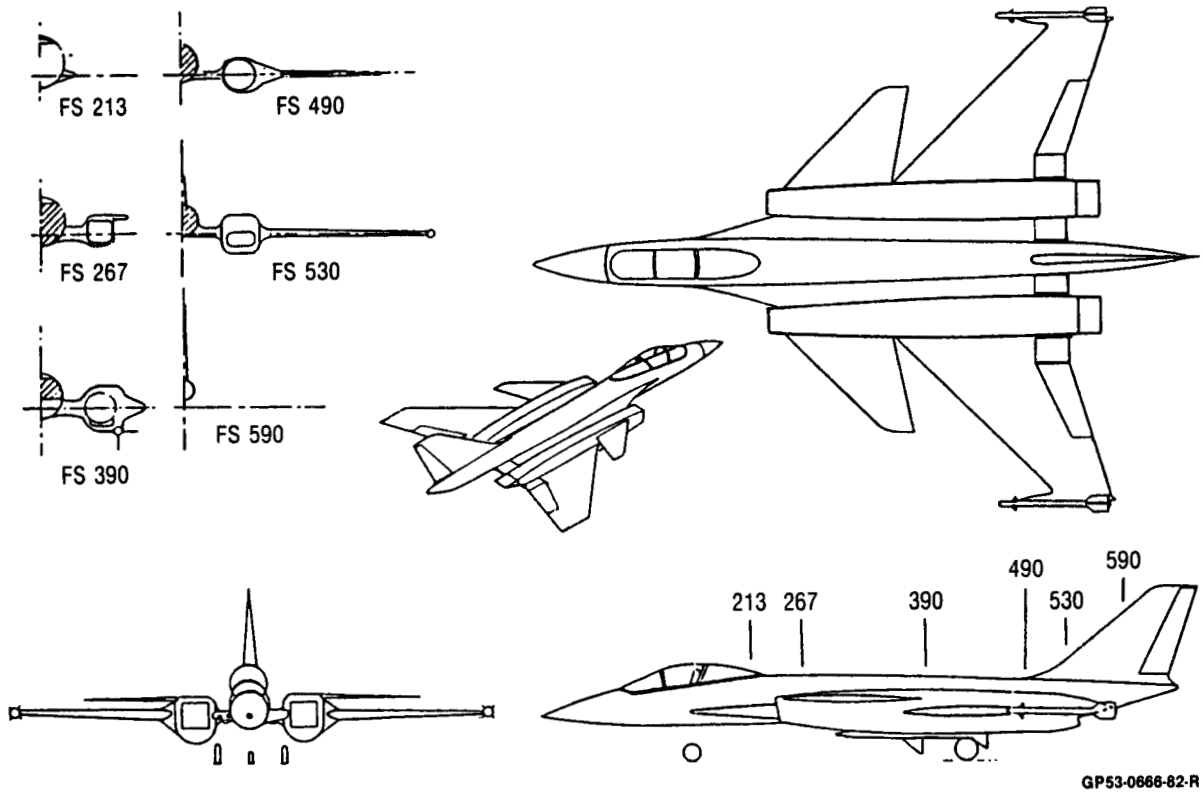

Figure 2-2. Air-to-Air Aerodynamic Configuration Developed in AFWAL/MCAIR Advanced Nozzle Concepts (ANC) Program

A comparison of the key geometry parameters of the scaled V/STOL configuration with the ANC model is provided in Figure 2-3. The ANC airframe parameters (i.e. wing, canard, fuselage, nacelle) are somewhat larger than would be required for the properly scaled V/STOL concept, as is the inlet capture area. The nozzle throat areas are essentially correct. The ANC inlet was therefore modified for the NASA program to reduce the capture area to the properly scaled value (35.23 cm^2 or 5.46 in^2).

	Supersonic V/STOL L+L/C Turbofan at 9.62% Scale	ANC Air-to-Air Model
Overall Fuselage Length	1.72 m (5.63 ft)	1.79 m (5.88 ft)
Nacelle Length	0.79 m (2.59 ft)	0.86 m (2.83 ft)
Wing Span	1.16 m (3.81 ft)	1.30 m (4.28 ft)
Wing Area	0.39 m^2 (4.15 ft^2)	0.48 m^2 (5.22 ft^2)
Canard Area	0.07 m^2 (0.79 ft^2)	0.09 m^2 (1.02 ft^2)
Inlet Capture Area	34.00 cm^2 (5.27 $in.^2$)	36.58 cm^2 (5.67 $in.^2$)*
Nacelle Maximum Area	107.75 cm^2 (16.7 $in.^2$)	116.14 cm^2 (18 $in.^2$)
Nozzle Throat Area (Dry)	18.65 cm^2 (2.89 $in.^2$)	19.42 cm^2 (3.01 $in.^2$)
Nozzle Throat Area (A/B)	32.78 cm^2 (5.08 $in.^2$)	33.23 cm^2 (5.15 $in.^2$)

*Modified to 35.23 cm^2 (5.46 $in.^2$) for NASA program

GP53-0666-69-R

Figure 2-3. Comparison of Key Geometry Parameters for Supersonic V/STOL System and ANC Model

An external geometry comparison of the modified (smaller inlet area) model and the lift plus lift/cruise V/STOL configuration at 9.62% scale, Figure 2-4, shows that the ANC model is an excellent representation of the V/STOL concept. The propulsion system components are properly scaled, as well as the relative location of the canard/inlet and wing/nozzle.

This NASA program investigated vehicle performance during the cruise and maneuver portions of a deck launched intercept mission. The lift engine was therefore not modeled during the test. The existing ANC ALBEN is aerodynamically similar to the full scale V/STOL ADEN at cruise and maneuver power settings. Therefore, the ALBEN was used for all testing in this NASA program.

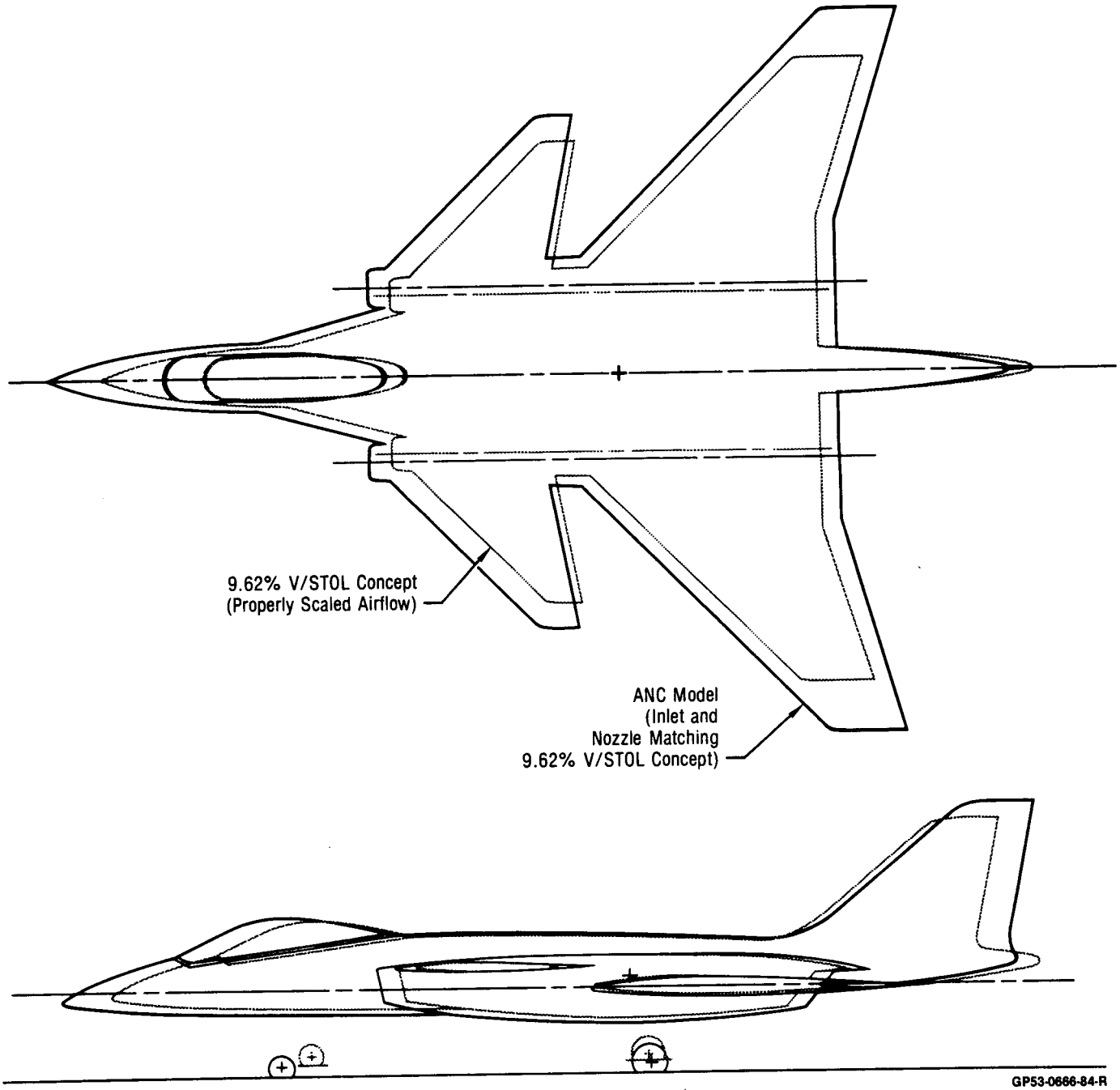

Figure 2-4. External Geometry Comparison Between ANC Model and 9.62% V/STOL Concept

3. TEST APPROACH AND MODEL DESCRIPTION

The overall test approach, model design, and associated data requirements were established to identify propulsion/airframe interactions using both the propulsion simulator and conventional model techniques. A major effort was made to ensure that any differences between the conventional and simulator mode test results were a true indication of propulsion/airframe aerodynamic coupling, as opposed to a bias error due to different methods of model design or data acquisition. To achieve this, model commonality was maximized in the CMAPS, Flow-Through, and Jet-Effects test modes.

An identical support system and metric arrangement were used in all test modes. A single internal balance measured all external aerodynamic forces except those on the exhaust nozzles, Figure 3-1. External pressures were measured to evaluate the nozzle aerodynamics. Common metric break locations and seal bridging mechanisms were also maintained, Figure 3-2.

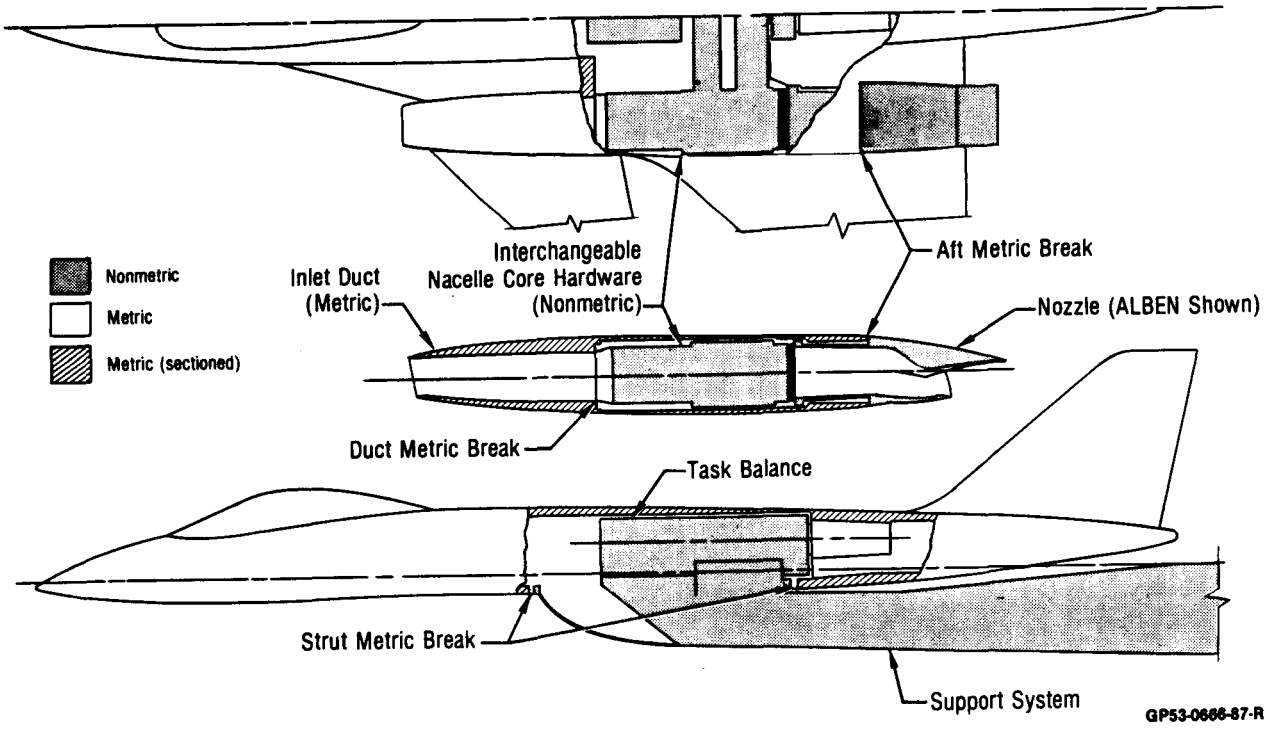

Figure 3-1. Common Support System and Metric Arrangement

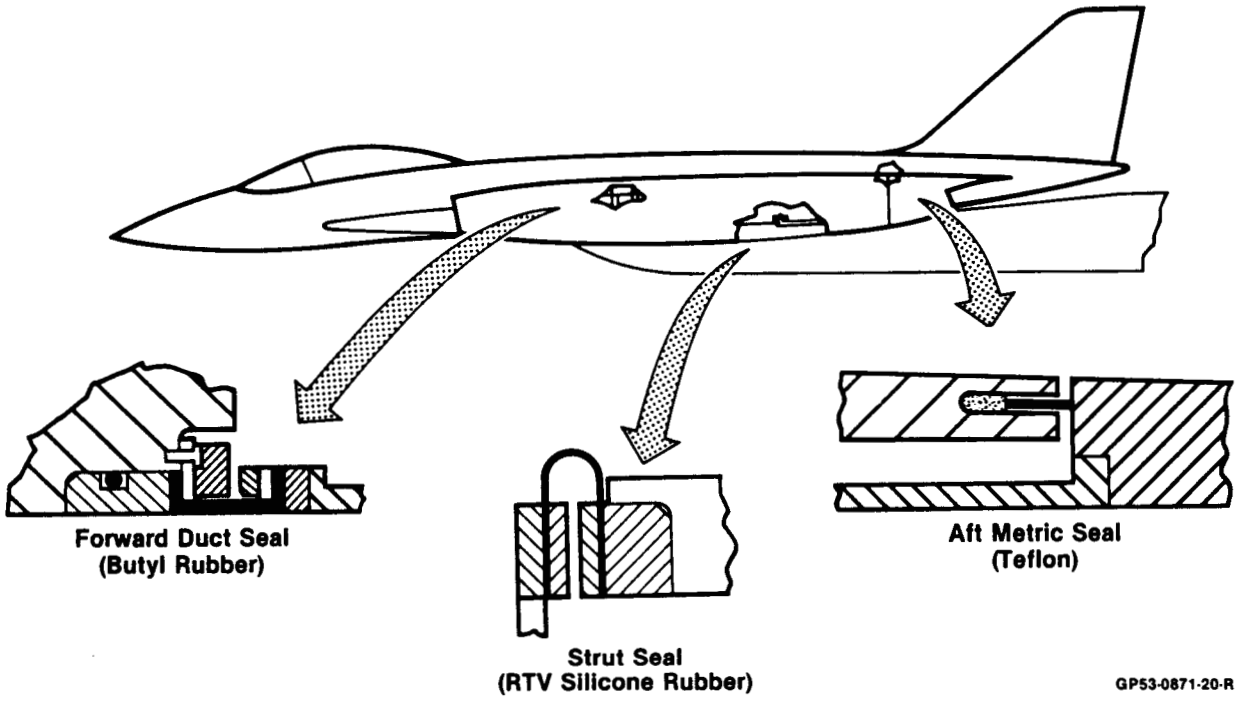

Figure 3-2. Metric Seal Details and Materials

The single model was designed to accept three different nacelle core hardware units. This allowed conversion to either CMAPS, Flow-Through, or Jet-Effects test modes by installing a simulator, jet-effects plenum, or flow-through duct inside the nacelle, as shown in Figure 3-3.

For all test modes, the model was instrumented to obtain the external aerodynamic characteristics of the airframe and the nozzles. The aerodynamic loads on the airframe were measured with a common 2.5 in. Task MK XXXII strain gauge balance. Thrust was not measured.

The non-metric ALBEN was instrumented with 49 external surface pressure orifices. The resulting surface pressures were used to perform a pressure-area integration from which lift, drag, and pitching moment on the nozzles were calculated. A total of 96 additional surface pressure measurements were provided on the wing, fuselage, and nacelle for diagnostic purposes.

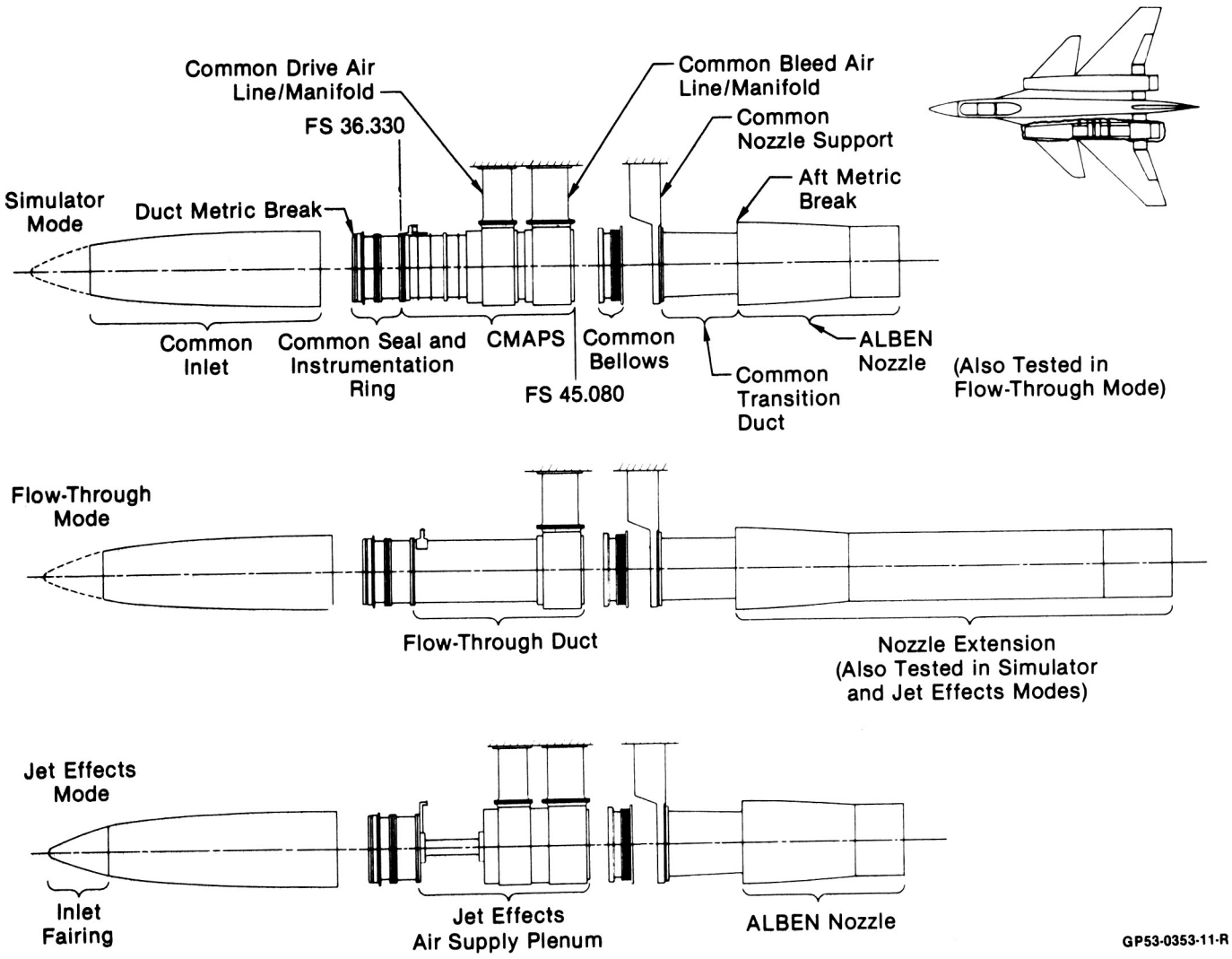

Figure 3-3. Test Mode Conversion Concept

A brief description of the wind tunnel model for each test mode is provided below. A more detailed description of the model is presented in Volumes II and III of this report (References 5 and 6).

3.1 CMAPS Mode

The major feature of the model is, of course, its ability to accept a CMAPS in each engine nacelle. In this program, the CMAPS units were always set to produce symmetric inlet and nozzle conditions left to right. However, each CMAPS was controlled

independently. The airflow paths through the simulator and the location of the engine instrumentation planes for the CMAPS are shown in Figure 3-4. High-pressure air, expanded through the CMAPS' single-stage turbine, drives a four-stage, axial-flow compressor. The turbine discharge air can be routed out of the CMAPS through a bleed line or mixed with the compressor airflow and exhausted through the nozzle. This approach makes it possible to simulate the inlet airflow and nozzle pressure ratio independently over a range covered by most current turbofan engines for supersonic fighters. The maximum achievable compressor airflow is 0.748 kg/sec (1.65 lb/sec), which equates to 80.74 kg/sec full scale (178 lb/sec). At this airflow, the CMAPS engine pressure ratio (EPR) can be varied from approximately 1.2 to 4.0. The simulator operating range for a nozzle in the afterburning position is shown in Figure 3-5.

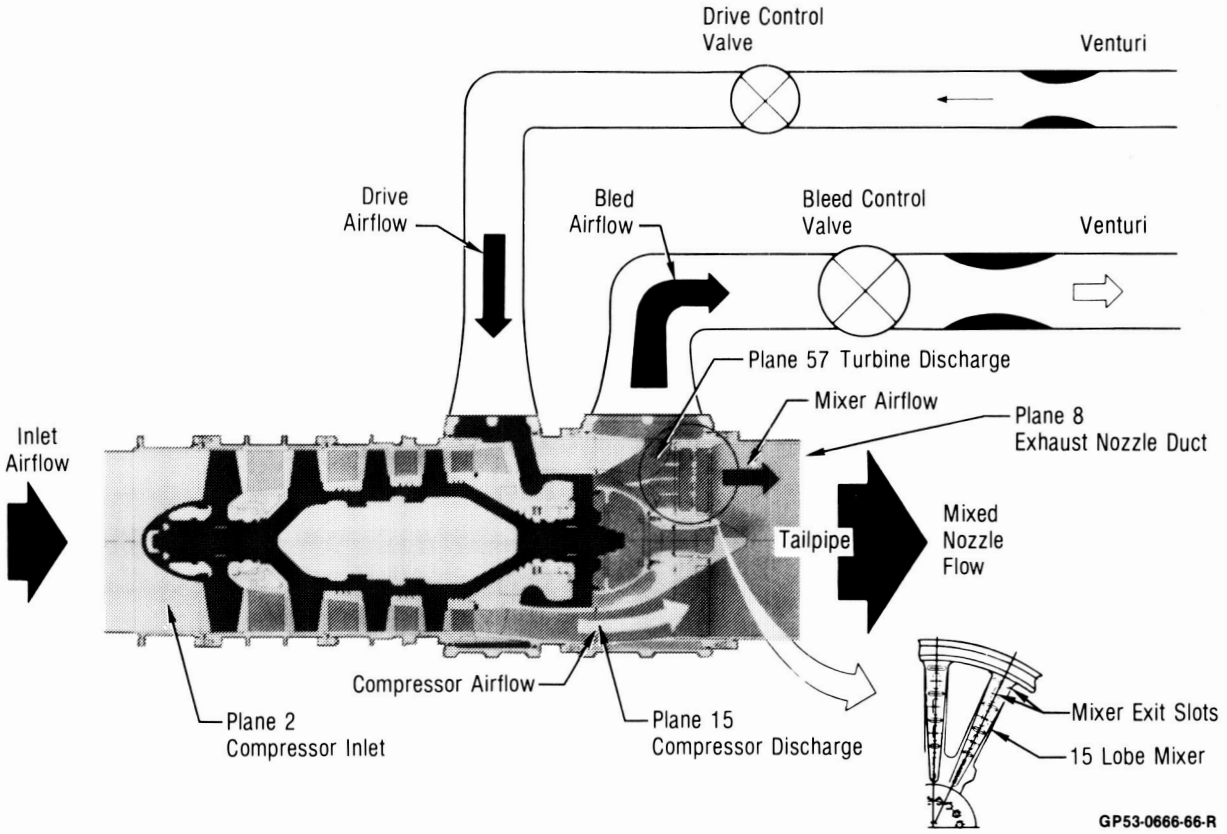

Figure 3-4. Simulator Internal Flow Paths

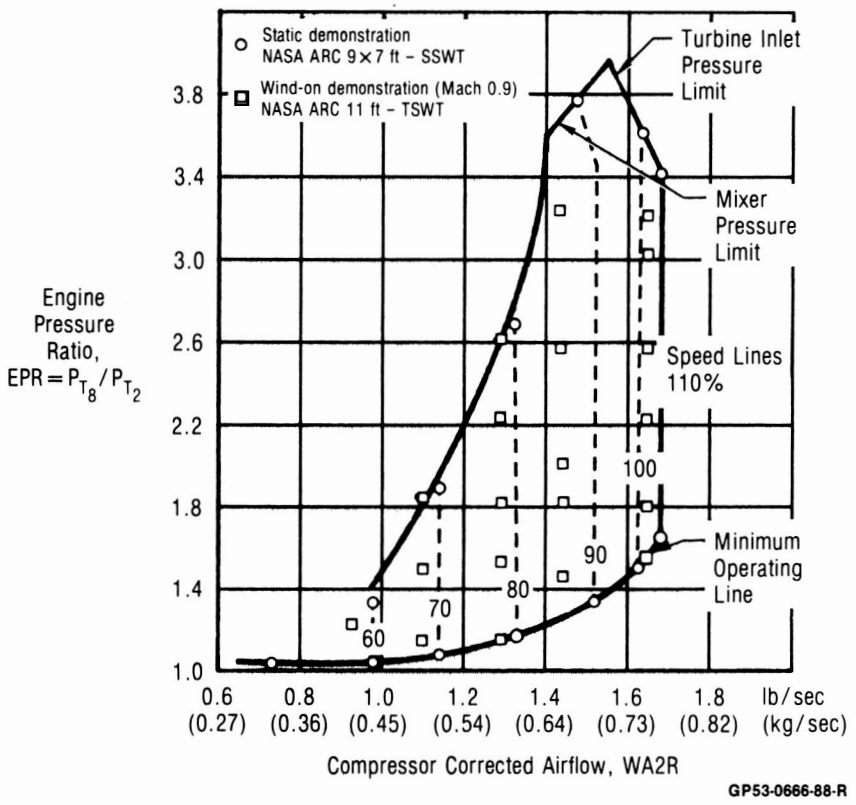

Figure 3-5. Demonstrated CMAPS Flexibility
A/B Power ALBEN

A detailed description of the CMAPS operation and performance is given by Wagenknecht and Bailey (References 8 and 9).

Pre-test static airflow calibrations of the CMAPS were conducted in the NASA ARC 9 x 7 ft. supersonic wind tunnel at NASA ARC. A photograph of both simulators mounted on the support sting during the airflow calibrations is shown in Figure 3-6. A calibrated bellmouth, shown on the right hand inlet in Figure 3-6, was used to determined the reference airflow. The airflow through the model was used to correct the balance outputs for axial stream thrust at the simulated enging face (Plane 2), and to determine inlet mass flow ratio (MFR) and ram drag.

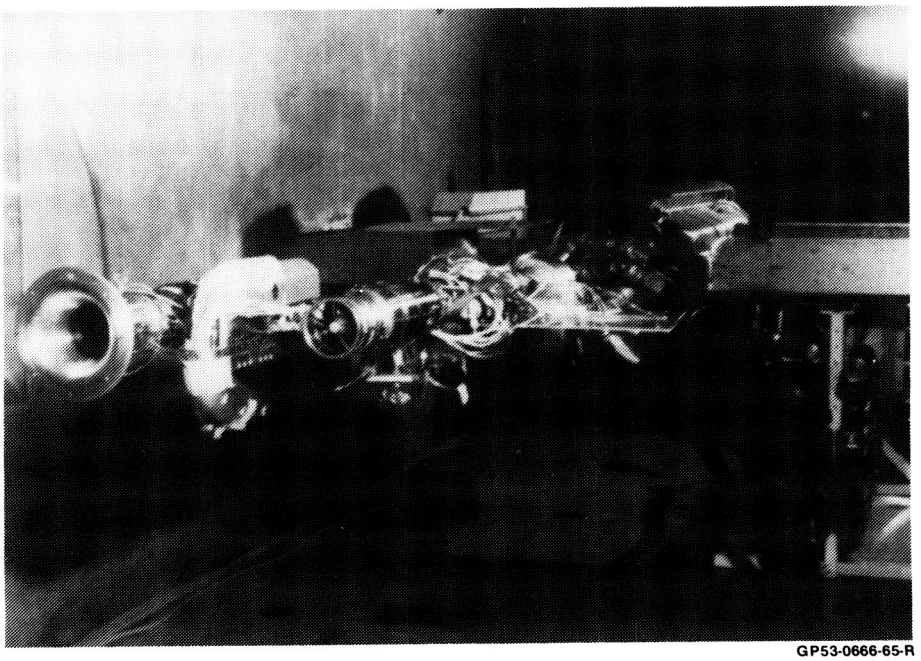

Figure 3-6. CMAPS Compressor Airflow Calibration Set-Up

The method used for CMAPS airflow calculation was based on static pressure at the turbine discharge (Plane 57) and rotor speed. Other methods of CMAPS inlet airflow calculation were also investigated based on measurements at the engine face (Plane 2), the compressor discharge (Plane 15), and the exhaust duct (Plane 8). However, the Plane 57 airflow calculation was shown to have the lowest uncertainty, as discussed in Reference 10 by S. C. Smith of NASA ARC.

3.2 FLOW-THROUGH MODE

During the Flow-Through mode, non-metric ducts replaced the simulators in the engine nacelles. The duct units were designed to model the propulsion simulators with respect to the internal inlet flow, particularly at the simulated engine face. Therefore, the Plane 2 instrumentation, inlet duct seals, and compressor face hubs were identical for Flow-Through and CMAPS modes.

3.3 JET-EFFECTS MODE

To achieve the Jet-Effects mode, plenum chambers were substituted for the simulators or flow-through ducts. The drive and bleed lines in the support sting furnished two independently controlled high pressure air sources to the plenum. The air was mixed in the plenum and exhausted through the ALBENs.

To maximize commonality between modes, this dual-flow plenum was designed to duplicate the internal airflow paths and resultant pressure and temperature patterns encountered in the CMAPS mode. Also, the inlet duct seal was retained during the Jet-Effects mode to maintain a common seal arrangement.

4. AERODYNAMIC TEST RESULTS

The net aerodynamic effect of flowfield interactions was investigated by comparing the basic CMAPS mode results with those obtained in the data build-up from the conventional mode. Any differences identified were attributed to inlet/nozzle flowfield coupling. The surface pressures and force and moment characteristics of discrete regions on the model were also analyzed to isolate the effects of any flowfield interactions.

4.1 TEST PROGRAM

The three test modes (CMAPS, Flow-Through, and Jet-Effects) required four externally different aerodynamic test configurations to identify the presence of flowfield coupling. These configurations were termed: 1) Simulated Aircraft, 2) Common Baseline, 3) Nozzle Extension, and 4) Nozzle Extension Baseline, Figure 4-1. The external differences in these configurations were only in the nacelle geometry; all other external model features were common. Aerodynamic increments from the last three configurations were combined to form the conventional mode data base.

To eliminate a possible bias due to different methods of inlet airflow measurement, the inlet/ airframe effects used in the conventional mode data build-up were obtained with CMAPS installed in the Nozzle Extension configuration, and again with the flow-through ducts installed. Therefore, the chosen method of inlet airflow calculation (Plane 57 method) was used in both conventional and CMAPS test techniques.

The four test configurations were derived from two inlet and two exhaust system configurations. The inlet could be tested either flowing or faired and the exhaust system could simulate either ALBENs or nozzle extension tubes with exit chokes. The extension tubes were used so the exhaust plume would not bias the effects of inlet mass flow ratio (MFR) on the metric airframe.

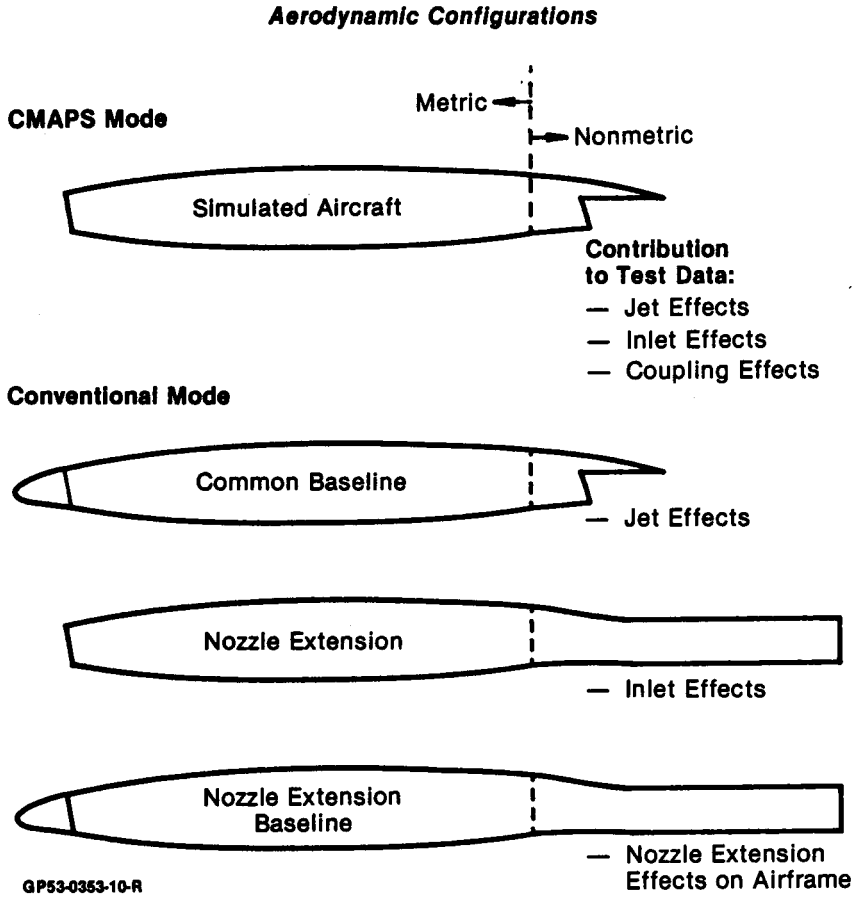

Figure 4-1. Comparison of Test Configuration

Four distinct nozzle configurations were tested in the Jet-Effects mode: unvectored dry power ALBEN and maximum afterburning (A/B) power ALBEN at 0°, 20°, and 30° thrust vectoring. However, in the subsequent CMAPS mode testing the unvectored A/B configuration was the only ALBEN tested due to a CMAPS O-ring failure. This prematurely ended testing in this mode. Therefore, all direct comparisons between conventional and simulator modes presented herein are based on the Simulated Aircraft configuration with unvectored A/B ALBENs.

The testing was performed from Mach 0.4 to Mach 1.4, up to 20° angle-of-attack, in the 11 ft transonic unitary plan wind tunnel at the NASA Ames Research Center, Moffett Field, California.

4.2 TOTAL AERODYNAMIC PERFORMANCE

In the CMAPS mode, the aerodynamic characteristics of the complete configuration were obtained directly at the actual inlet/nozzle operating conditions. This was possible because the propulsion simulators permitted the simultaneous matching of the inlet and nozzle flow conditions at the desired operating points.

The total aerodynamic performance characteristics from the conventional mode are based on a build-up of data from three separate configurations, as previously noted. The three conventional mode configurations were combined using the force and moment accounting procedure shown in Figure 4-2. The basic airframe aerodynamics, which included inlet/airframe interactions (i.e. MFR effects) but not nozzle/airframe interactions, were obtained from the metric portion of the Nozzle Extension configuration. The effect of the nozzle extensions on the airframe aerodynamic characteristics was obtained as the difference between the jetoff Common Baseline and Nozzle Extension Baseline configurations.

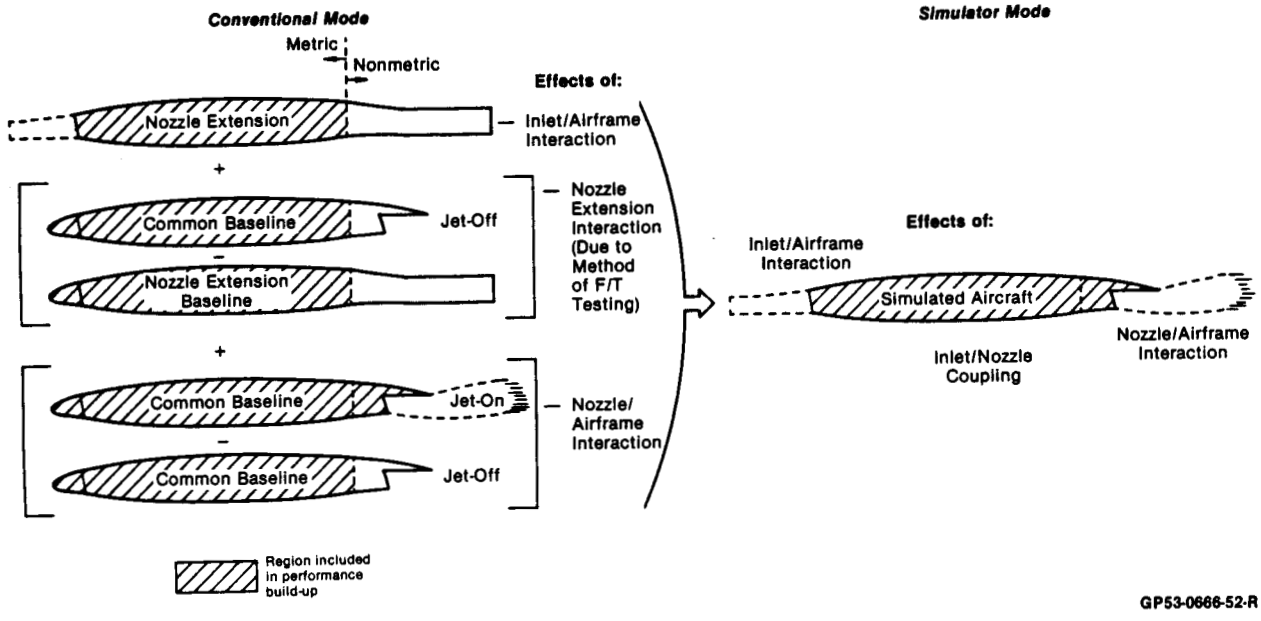

Figure 4-2. Aerodynamic Accounting Procedure

Finally, the nozzle/airframe interactions, including operating NPR effects, were obtained as the difference between jet-on and jet-off runs of the Common Baseline configuration in the JetEffects mode.

During the build-up, the conventional mode data were adjusted to the same MFR, NPR and angle-of-attack as the basic CMAPS mode data. These small adjustments were obtained by interpolation.

The largest differences in aerodynamic performance between the CMAPS and conventional modes occurred supersonically. As shown in Figure 4-3, the simulator technique demonstrated nearly 20 counts (one "count" is equal to D/qS_W = 0.0001) less drag than the conventional mode build-up at a constant lift coefficient.

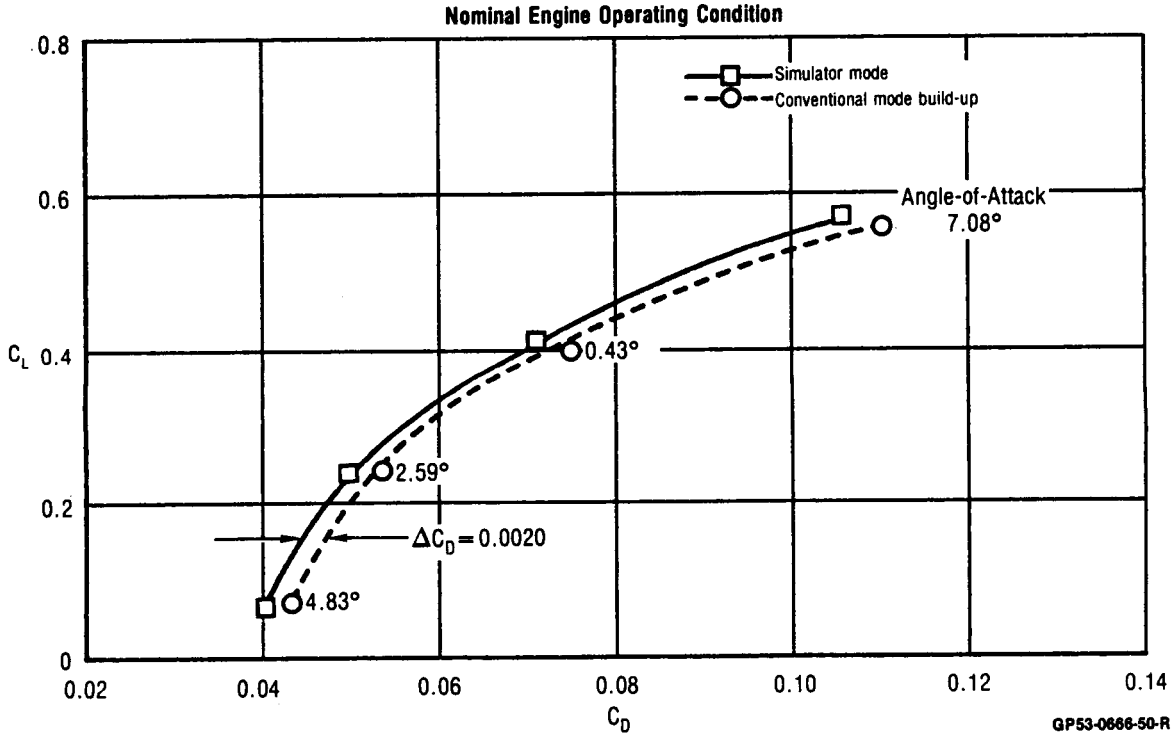

Figure 4-3. Drag Polar Comparison
- **Simulator vs Conventional Mode**

Mach 1.4 Canard Angle = 0°
Mass Flow Rotation = 0.793 Nozzle Pressure Ratio = 9.60

The effects of these interactions can also be seen in the trends of drag versus NPR. As shown in Figure 4-4, the basic Jet-Effects mode results can be incremented by the flowing inlet effects and nozzle extension effects to obtain the conventional mode build-up. The basic assumption in such a build-up is that the inlet/airframe effects are independent of NPR. The conventional build-up curve is thus parallel to the basic Jet-Effects curve. Any differences between the CMAPS and built-up conventional mode curves is an indication of flowfield coupling. This includes differences in shape, as well as magnitude. Supersonically, the CMAPS mode predicts a nearly constant increment of 20 counts less drag than the conventional mode.

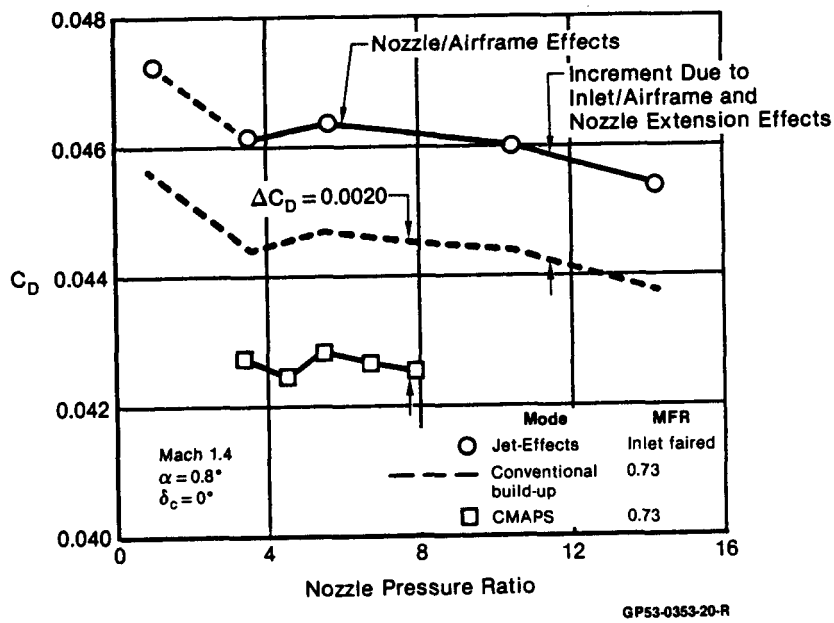

Figure 4-4. Effect of Flowfield Coupling on Full Configuration Drag at Mach 1.4

Subsonically, the simulator technique generally exhibits lower lift and drag than the conventional technique at a given angle-of-attack. However, the drag polars from the two techniques nearly coincide, Figure 4-5.

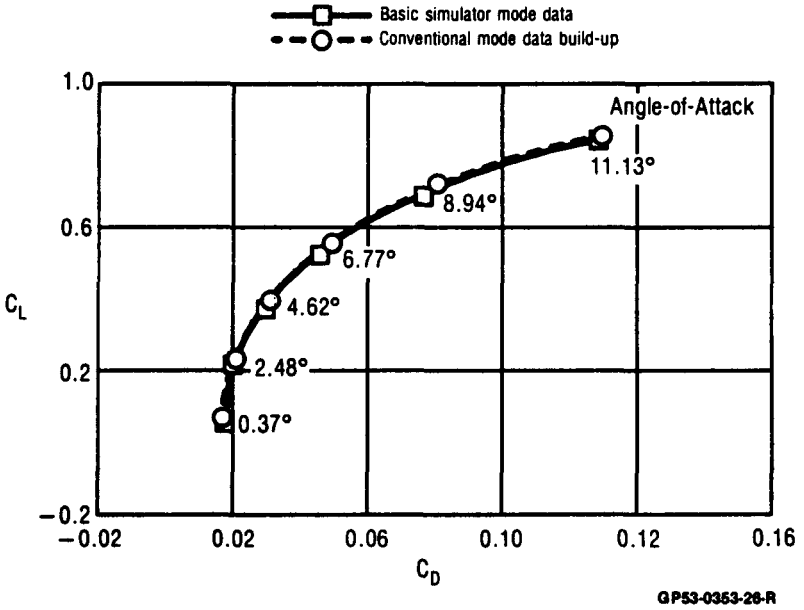

Mach 0.6 Canard Angle = −5°
Mass Flow Ratio = 0.916 Nozzle Pressure Ratio = 3.86

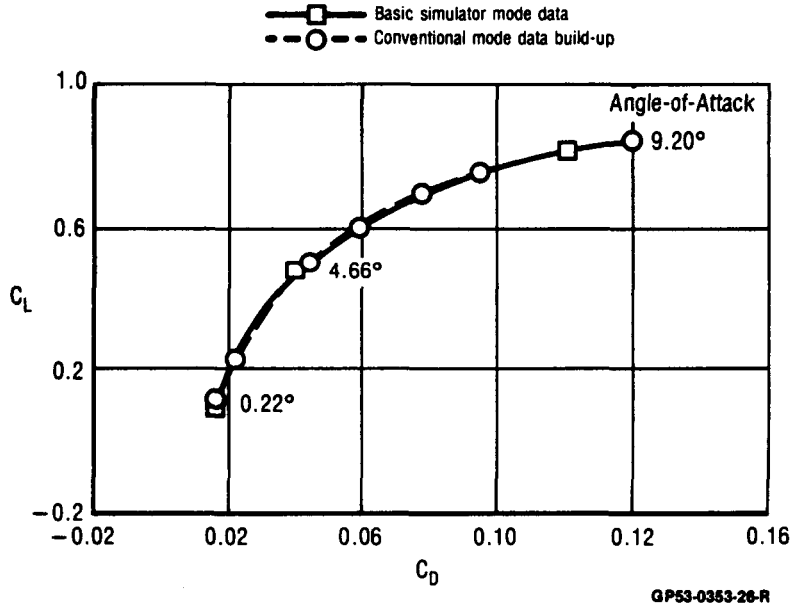

Mach 0.9 Canard Angle = −5°
Mass Flow Ratio = 0.753 Nozzle Pressure Ratio = 5.30

Figure 4-5. Drag Polar Comparison Simulator vs Conventional Mode

Further evidence of subsonic interactions are seen in the trends of drag versus NPR at Mach 0.6 and 0.9, Figure 4-6. In this case, the flowfield interactions are reflected as a difference in shape between the CMAPS and conventional mode curves.

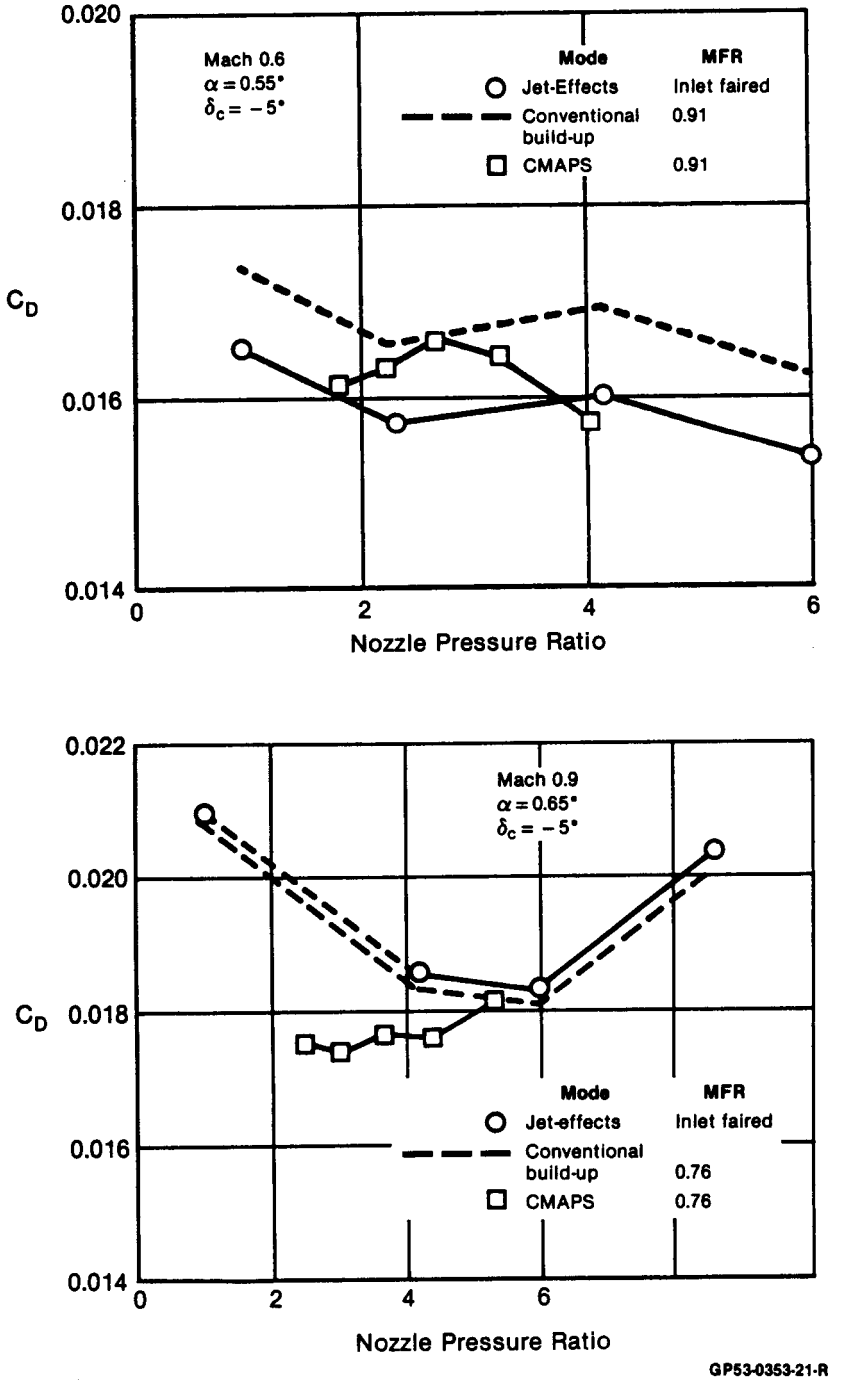

Figure 4-6. Effect of Flowfield Coupling on Full Configuration Drag

Comparison of total aerodynamic performance from CMAPS and conventional mode testing, as presented above, indicates the net effect of any flowfield coupling which may occur. However, localized flowfield coupling may exist which affects only discrete aircraft components and not the overall performance.

4.3 LOCAL FLOWFIELD INTERACTIONS

Localized flowfield interactions were identified by analyzing the surface pressures and force and moment characteristics of specific regions on the model. The most significant localized interactions were observed on the nozzles and the nacelle upper surface.

The largest differences in pressure-area integrated nozzle drag between the Jet-Effects and CMAPS modes occurred supersonically. As shown in Figure 4-7, the CMAPS mode with flowing inlets exhibits from 6 to 12 counts less nozzle drag than the corresponding Jet-Effects mode with faired inlets. A constant incremental difference in drag would be expected if the inlet fairing produced a bias error. However, the changes in slope or shape of the drag coefficient curve in Figure 4-7 indicate that flowfield interactions exist. In this example, the difference between the maximum inlet fairing bias and the minimum bias is 6 drag counts due to inlet/nozzle flowfield coupling.

Evidence of flowfield coupling on the nozzle was also seen subsonically. As shown in Figure 4-8, the magnitude of the nozzle drag for each test technique is nearly the same. However, the trends with NPR are again different. In this comparison, the CMAPS mode demonstrates from 2 counts more drag to 6 counts less drag than the Jet-Effects mode.

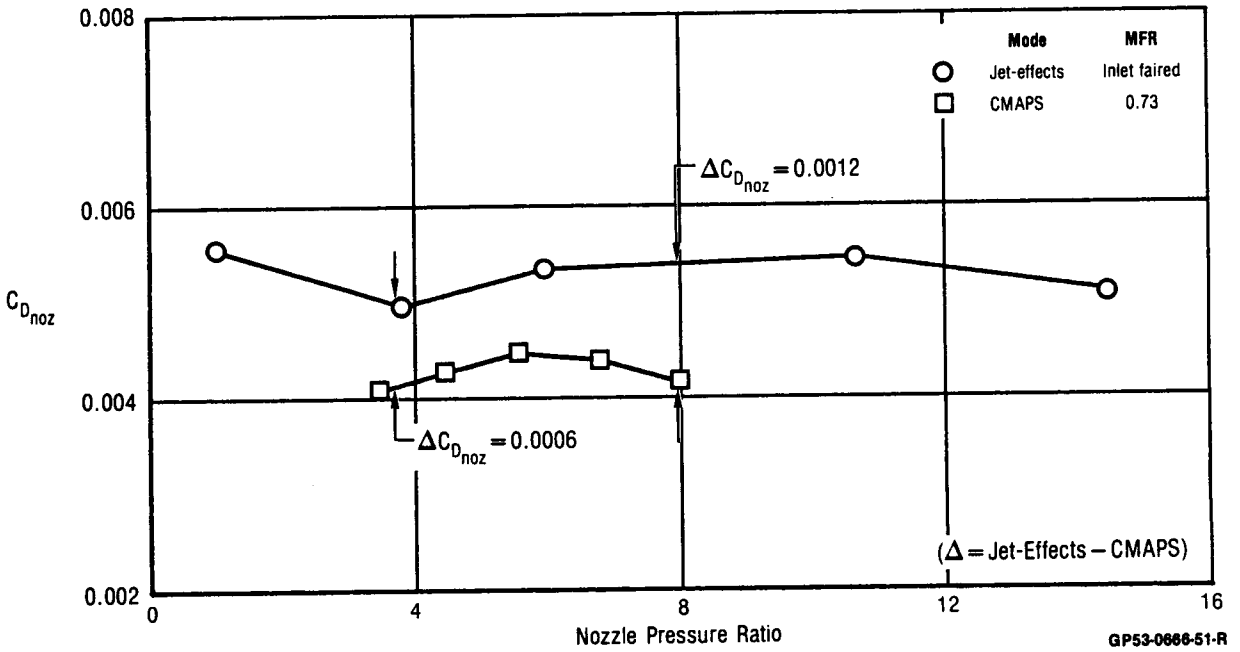

Figure 4-7. Effect of Flowfield Coupling on Nozzle Drag
Mach 1.4 $\alpha = 0.8°$ $\delta_C = 0°$

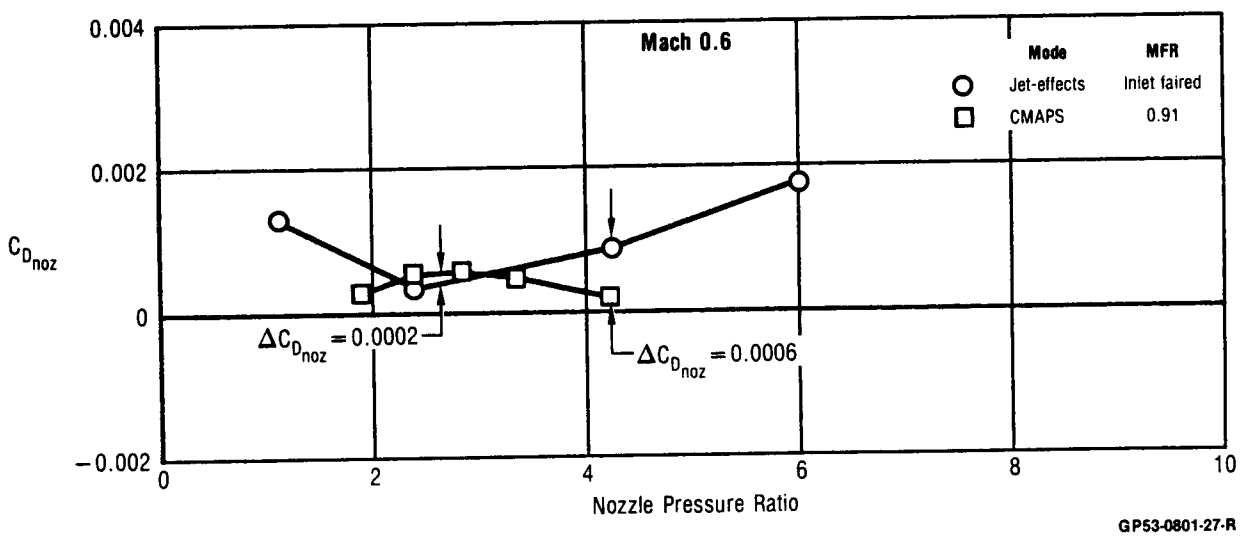

Figure 4-8. Flowfield Coupling Effects on Nozzle Drag
Subsonic Conditions $\alpha = 0$ $\delta_C = -5°$

The differences between the CMAPS and Jet-Effects mode nozzle drags presented above are attributed to inlet flowfield differences affecting the nozzle flowfield. In this case, the comparison was between a flowing and a faired inlet. The inlet fairing effect on jet-on nozzle drag is a bias error inherent to conventional mode testing.

A traditional method of addressing this bias error is to determine a drag increment between a reference nozzle operating at a very low flow- through NPR (or a solid sting plume simulation) and the correct nozzle geometry operating at the engine operating NPR. However, this approach properly accounts for the inlet fairing bias only at the very low flowthrough NPR. It assumes that the inlet fairing bias is constant and does not affect the relationship between nozzle drag and NPR. In the presence of inlet/nozzle flowfield coupling, this assumption is not necessarily correct, as shown in Figures 4-7 and 4-8.

Another flowfield interaction effect investigated was the variation of nozzle drag with MFR and NPR, over a specific canard angle range. The comparison shown in Figure 4-9a, at constant MFR and increasing NPR, indicates a nearly constant incremental change in nozzle forces. This increment is thus a constant throttle-dependent effect on the nozzles and is not considered an indication of inlet/nozzle interactions. However, a decrease in MFR for a constant NPR, Figure 4-9b, changes the basic shape of the curves. This change in trend indicates that the inlet flowfield is acting through the canard to affect the nozzle flowfield.

The data presented in Figure 4-9 also indicates that the canard alone interacts with the nozzle flowfield, regardless of MFR and NPR. This is interesting because the approach for conventional testing is to assume that the effects of the canard on nozzle drag are negligible. Of course, this type of interaction could be obtained with traditional Jet-Effects mode testing by imposing canard angle variations.

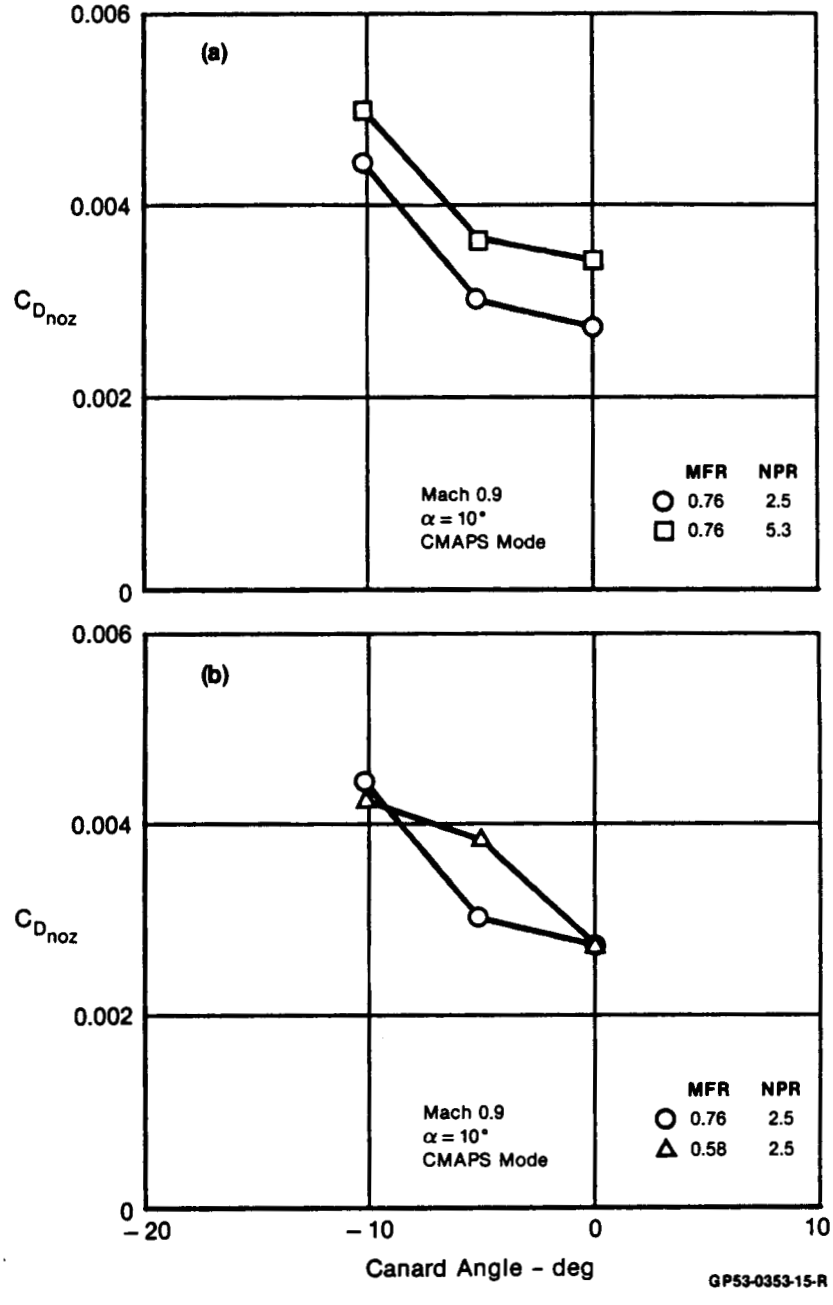

Figure 4-9. Inlet/Canard Effects on Nozzle Drag

These same canard/nozzle interactions were not observed at lower subsonic speeds. As shown by CMAPS mode data at Mach 0.6, Figure 4-10, there is essentially no variation of nozzle drag with canard angle at angles-of-attack of 0° or 9°. This same trend was also identified on the jet-off, Common Baseline configuration, Figure 4-11. The nozzle drag is affected by canard angle deflection at Mach 0.9 but not at Mach 0.4 and 0.6.

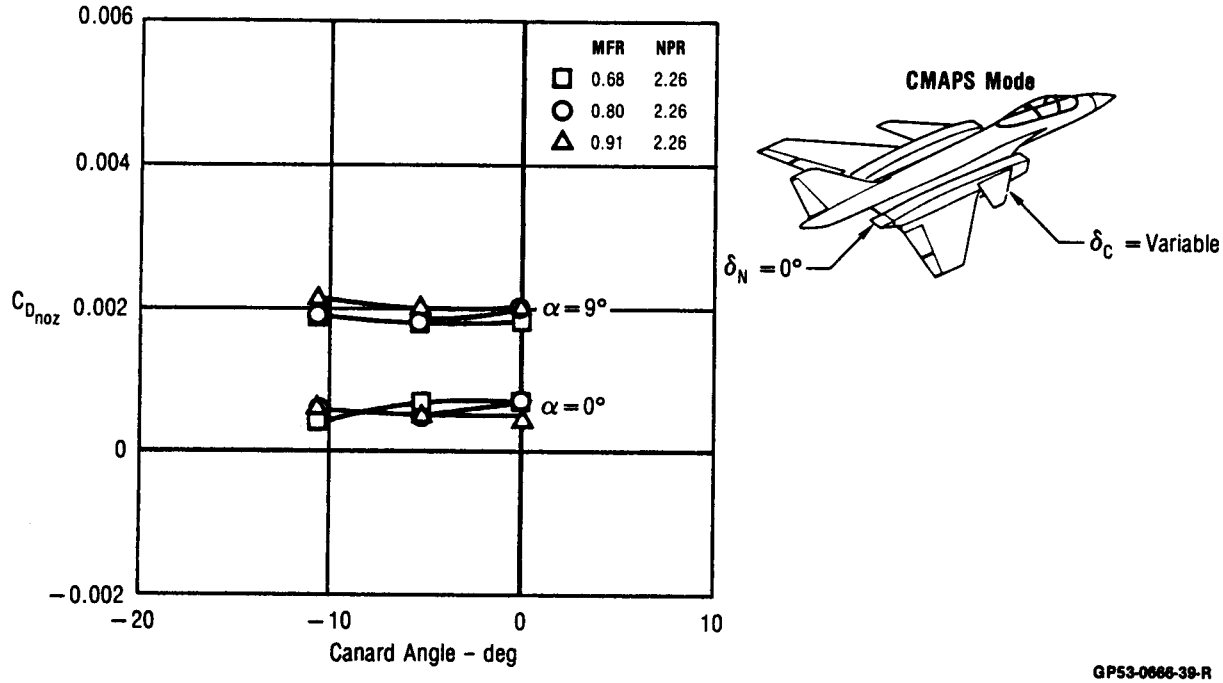

Figure 4-10. Inlet/Canard Effects on Nozzle Drag
Mach 0.6

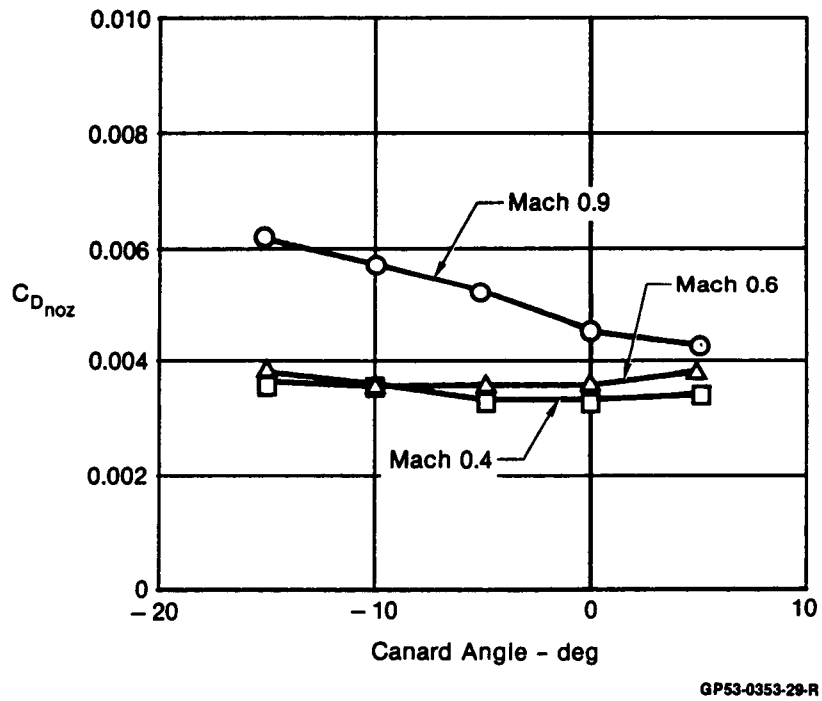

Figure 4-11. Effect of Mach Number on Canard/Nozzle Aerodynamic Coupling
Jet-Off - Common Baseline Configuration
α = 9°

The data suggests that this coupling phenomena may be due to unstable flowfield characteristics associated with transonic flow. Within this regime, shock waves can form and move along the wing, nacelle, and nozzle in response to canard angle variations. At Mach numbers above or below this transonic regime, the flowfield is sufficiently stable that canard variations do not significantly influence the nozzles.

Variations in nacelle surface pressure distributions also indicate the interaction of forward and aft flowfields. The largest indications of such inlet/nozzle flowfield interactions were seen in comparisons of faired and flowing inlet configurations. As shown in Figure 4-12, the presence of the fairing is felt over the entire length of the nacelle and nozzle. However, at a higher NPR, the fairing effects on the nozzle pressures diminish, Figure 4-13. These trends are typical of the subsonic results, and indicate that the inlet condition (flowing or faired) impacts the flowfield around the nozzles. These results substantiate the trends of subsonic nozzle drag with NPR variations presented earlier. Similar inlet fairing effects were also identified supersonically.

The effects of aerodynamic coupling identified here could be greater for other propulsion system geometries. For example, a vectored or dry power nozzle configuration could present an even higher potential for inlet/nozzle flowfield coupling than the tested unvectored A/B configuration. The smaller exit area of a dry power nozzle results in much more aft-facing projected area than an A/B geometry. Further, the effects of vectored thrust have been shown to propagate farther upstream than those of unvectored thrust (Reference 3).

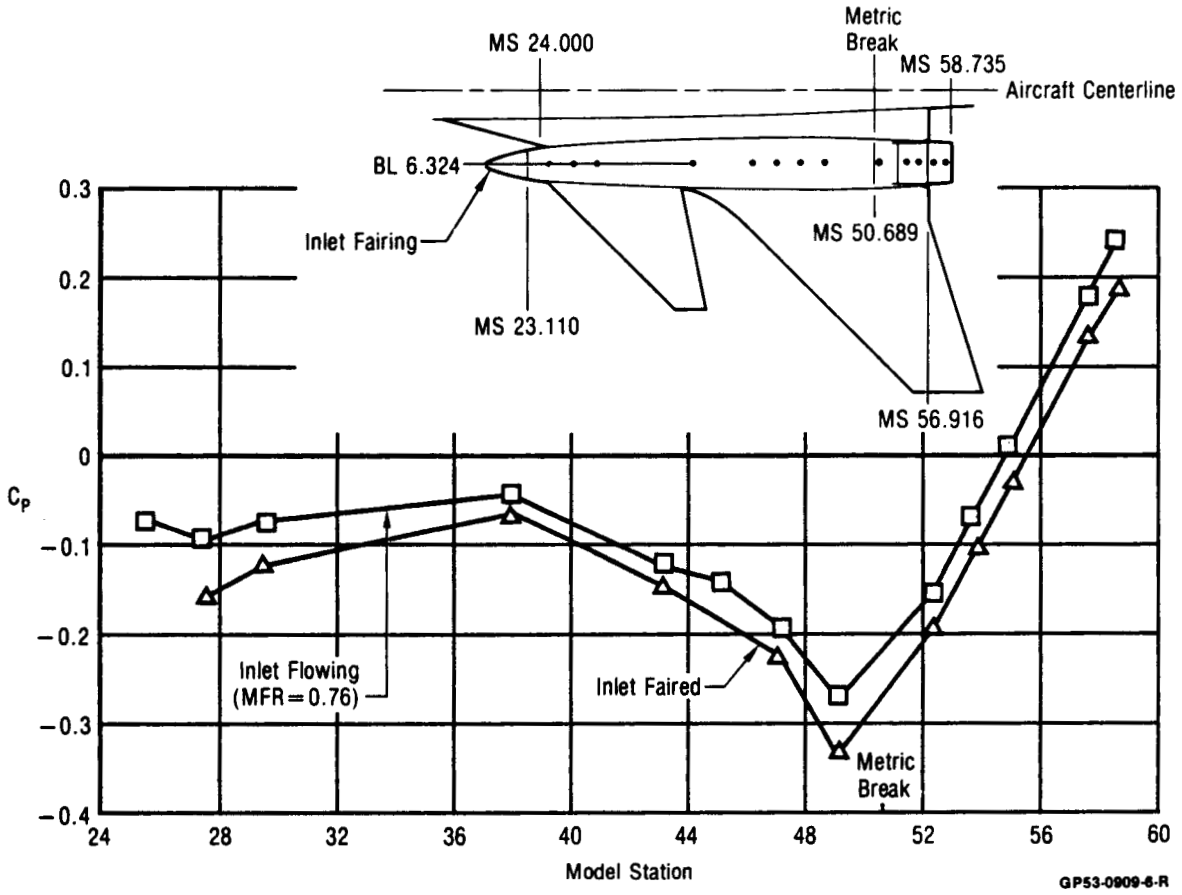

Figure 4-12. Inlet Fairing on Nacelle Upper Surface Pressure Distribution at Mach 0.9
$\alpha = 0°$ $\delta_C = -5°$ NPR = 4.2

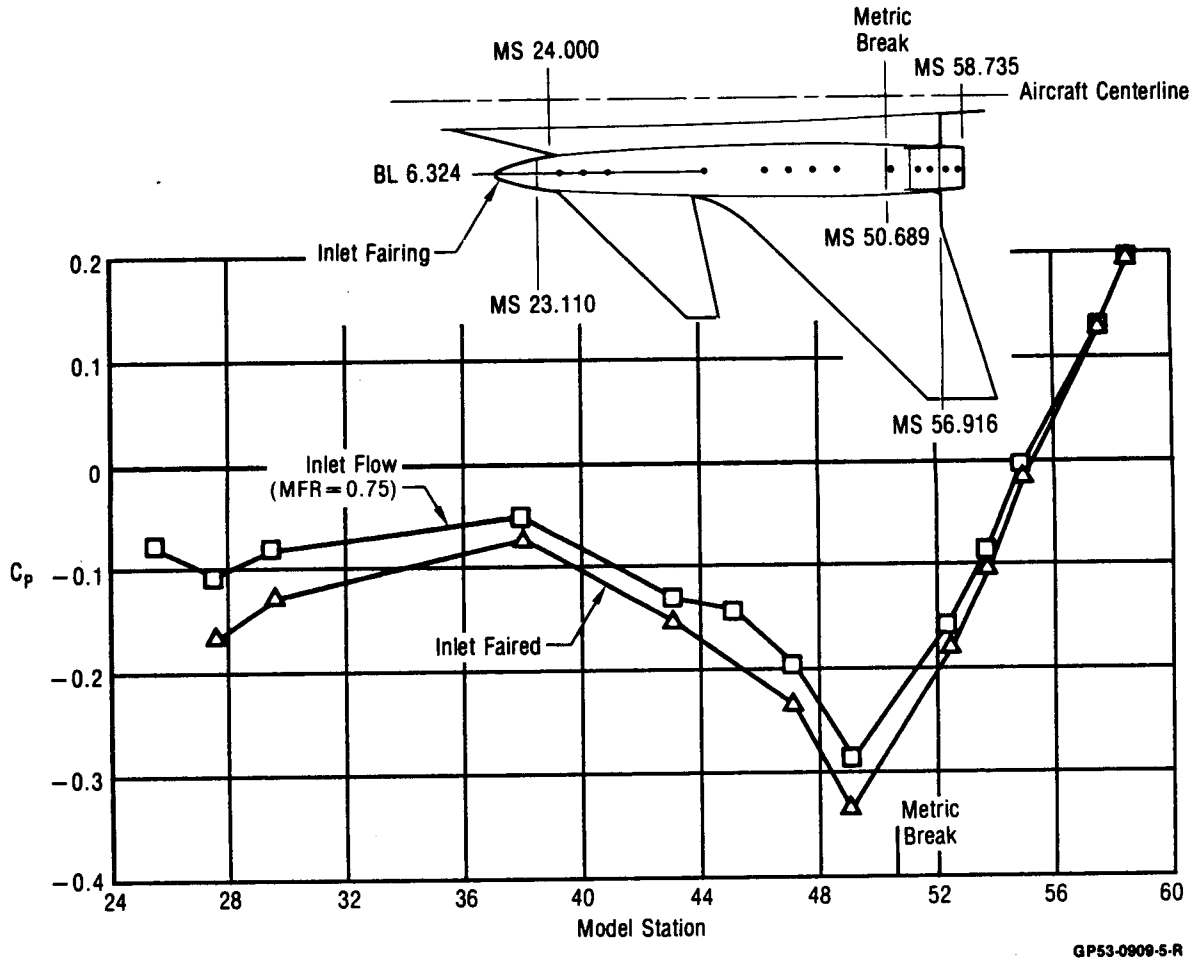

Figure 4-13. Inlet Fairing on Nacelle Upper Surface Pressure Distribution at Mach 0.9
$\alpha = 0°$ $\delta_C = -50°$ NPR = 5.6

5. CMAPS UTILIZATION

The experience gained during the design, calibration, and testing of the CMAPS-equipped model is as important as the aerodynamic test results. Requirements in model design and calibration require additional considerations compared to conventional wind tunnel models. The operation of the simulators in a wind tunnel environment was found to be generally reliable, but specific areas will require further development. The operational experience gained during this program is therefore reviewed, and effort recommended for continued development of propulsion simulators.

5.1 MODEL DESIGN CONSIDERATIONS - Wind tunnel models designed to accept the current propulsion simulators are subject to various constraints not usually present for conventional models. These constraints result from the physical size of a CMAPS, the available balance systems, and the drive and bleed line airflow/temperature extremes. Special considerations must therefore be made regarding model scale, metric break arrangement, support system type, and balance temperature control.

5.1.1 Model Scale - The physical size and airflow capabilities of the existing propulsion simulators dictate the scale of the wind tunnel model. The physical size is obviously important in determining scale factor since the units must fit inside the model. Since a CMAPS is a tool for propulsion system testing, the model's scaled airflow must also match full scale engine capability.

Characteristic dimension and airflow parameters which are common to both propulsion simulators and full-scale engines are used in the scaling exercise. The diameter of the compressor face is the primary characteristic dimension for scaling to spatial constraints. The scale factor equation based on compressor face diameter is simple:

$$\text{Scale Factor}_{\text{DIAMETER}} = \frac{\text{CMAPS COMPRESSOR FACE DIAMETER}}{\text{ENGINE COMPRESSOR FACE DIAMETER}}$$

The maximum corrected airflow is the characteristic parameter for scaling to airflow capability. The scale factor equation based on airflow is:

$$\text{Scale Factor}_{\text{AIRFLOW}} = \frac{\text{MAX CMAPS COMPRESSOR CORRECTED AIRFLOW}}{\text{MAX ENGINE CORRECTED AIRFLOW}}$$

Ideally, both size and airflow considerations would generate the same model scale. Unfortunately, this is not often the case when existing full-scale engines are scaled to the propulsion simulator. A comparison of several current and advanced engines scaled to the CMAPS' size and airflow is presented in Figure 5-1. As shown, the model scale based on airflow is often less than that based on dimensional constraints. This situation could obviously result in difficulty in physically fitting the simulators inside a model which is properly scaled for airflow.

Engine	W_2 Corrected Design kg/sec (lbm/sec)	D_2 m (in.)	Scale Airflow (percent)	Scale Diameter (percent)
CMAPS	0.748 (1.65)	0.0762 (3.0)	—	—
F100-PW-100	102.8 (226.7)	0.884 (34.8)	8.53	8.62
F100-PW-220	100.9 (222.5)	0.884 (34.8)	8.61	8.62
PW 1128	110.0 (242.5)	0.884 (34.8)	8.25	8.62
PW 5000	113.9 (251.0)	0.905 (35.6)	8.11	8.43
F110-GE-100	119.4 (263.2)	0.913 (35.95)	7.92	8.34
F404-GE-400	64.2 (141.5)	0.709 (27.9)	10.80	10.75
PW Lift/Cruise Turbofan	80.8 (178.0)	0.770 (30.3)	9.62	9.90

GP53-0801-14-R

Figure 5-1. Current and Advanced Engines Scaled to CMAPS by Airflow and Compressor Diameter

Scaling for the present program illustrates a possible approach. The lift/cruise turbofan engine selected for the study configuration of this program is included in the table of Figure 5-1. Scaling for this engine indicates the scale factor based on compressor face diameter (9.90%) to be greater than that based on airflow (9.62%). Since this program was intended to identify inlet/nozzle flowfield coupling, the properly scaled airflow was required. The physical installation of simulators in the model was not a problem because an adequate CMAPS envelope was provided when the model was originally fabricated for the ANC program (Reference 3). However, this approach resulted in a model for the NASA program which was somewhat larger than the study vehicle scaled to 9.62%. The properly scaled airflow was maintained by scaling down the existing inlet slightly to the 9.62% size, as previously discussed in Section 2.2.

Although not a constraint for this NASA program, the overall length of the CMAPS/nozzle assembly may impact the scale of simulator powered models which represent more compact aircraft designs. The distance from the compressor face to the nozzle throat is a characteristic dimension for scaling to overall length. An example of scaling to CMAPS length as compared to airflow and engine face diameter is presented in Figure 5-2 for an advanced General Electric engine. It may be difficult to install a simulator with the tailpipe/nozzle assembly used in this program inside a model sized to the airflow of the advanced engine depicted in Figure 5-2. In such a case, some of the extra length needed for the CMAPS installation may have to be gained in the inlet diffuser duct or the augmentor.

It should be noted however, that shorter CMAPS/tailpipe/nozzle assemblies are possible. The shortest feasible length is 31 cm (12.25 in.) which would translate into a model scale of 10.1% for the advanced engine in our example.

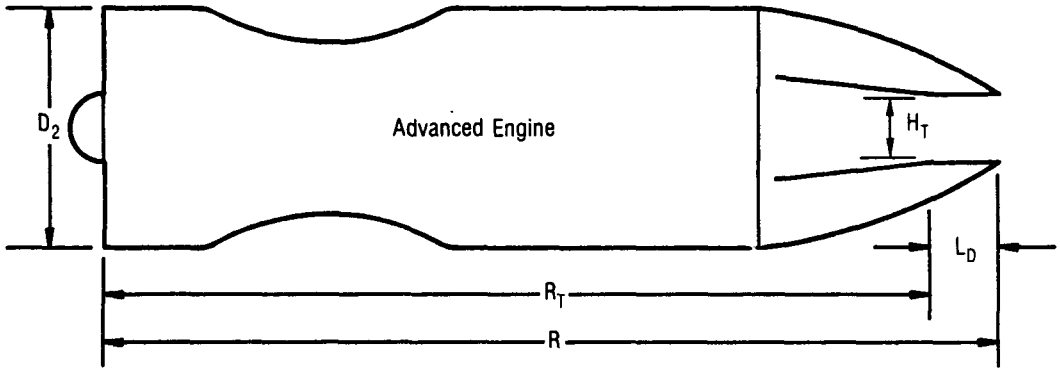

Advanced Engine:

W_{2R} = Design Corrected Airflow: 102 kg/sec (226 lbm/sec)

D_2: 89.9 cm (34.4 in.)

R: 257.4 cm (140.7 in.)

Assume A Nozzle to Calculate "R_T":

$L_D/H_T = 2.0$ @ Dry Power

AR = Aspect Ratio = 4

A_t = Throat Area = 2445 cm^2 (379 $in.^2$) @ W_{2R} = 102 kg/sec

$AR = A_T/H_T^2 = 4 \Rightarrow H_T = 24.7$ cm (9.73 in.)

$L_D/H_T = 2 \Rightarrow L_D = 49.4$ cm (19.5 in.)

$\therefore$ For This Engine/Nozzle $\Rightarrow R_T = 308$ cm (121.3 in.)

For CMAPS/Nozzle in This Test $\Rightarrow R_{T_C} = 48$ cm (18.9 in.)

	Scale to Length:	Scale to Diameter:	Scale to Airflow:
Scale Factor =	$\frac{48 \text{ cm}}{308 \text{ cm}}$	$\frac{7.6 \text{ cm}}{89.9 \text{ cm}}$	$\sqrt{\frac{0.75 \text{ kg/sec}}{102 \text{ kg/sec}}}$
$\Rightarrow$	15.6% Scale	8.5% Scale	8.6% Scale

GP53-0801-15-R

Figure 5-2. Scaling Model to Length of CMAPS/Nozzle Assembly

5.1.2 Metric Arrangement - CMAPS-equipped models can be designed for any of the metric arrangements traditionally used with conventional Jet-Effects and Flow-Through models. However, many of the conceivable metric arrangements may be difficult to implement for a CMAPS model due to model volume constraints or metric break tare considerations.

The metric arrangements are of two major categories; metric and non-metric CMAPS installations. Typical metric arrangements with related comments are shown in Figure 5-3. Each arrangement designed with metric CMAPS requires bridging a balance with at least two high pressure air lines. It would be difficult to install conventional, "off-the-shelf" wind tunnel balances and metric air-transfer systems inside a properly scaled wind tunnel model to meet this requirement. This situation could possibly be solved with a self-contained, balance/air-transfer apparatus. However, such a system does not yet exist to our knowledge. NASA-Ames is currently pursuing the conceptual design of a "flow-through" balance to fill this void.

Metric CMAPS installations will also require a thrust calibration in order to calculate thrust-removed drag during a wind tunnel application. Such thrust calibrations can be conducted in the NASA-Ames Propulsion Simulator Calibration Laboratory (PSCL) following its scheduled completion in 1986, Reference 11.

The concepts with non-metric simulators, or those with metric simulators on a multiple balance system, require calculation of stream thrust at the metric break locations. These locations are either forward of the CMAPS compressor face or aft of the CMAPS mixer, or both, depending on the arrangement. Such a calculation can be accurately performed at the compressor face metric break with a reasonable amount of total/static pressure instrumentation at that plane. The same calculation at a metric break downstream of the mixer would require an unusual amount of instrumentation to account for the high levels of pressure and temperature distortion. Therefore, concepts which propose a metric break between the CMAPS and tailpipe/nozzle assembly are discouraged.

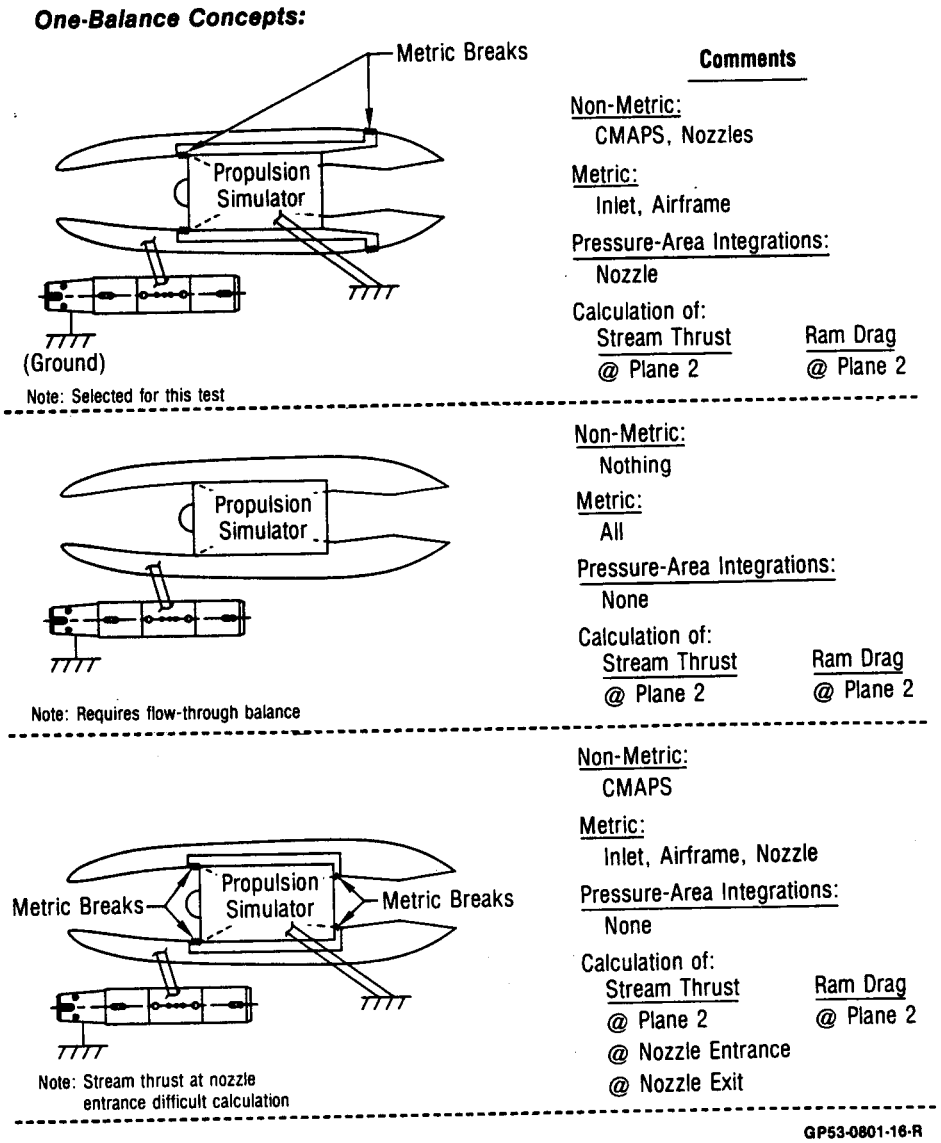

Figure 5-3. Typical Metric Arrangements for CMAPS - Equipped Models

Two Balance Concepts
With No Pressure-Area Integrations:

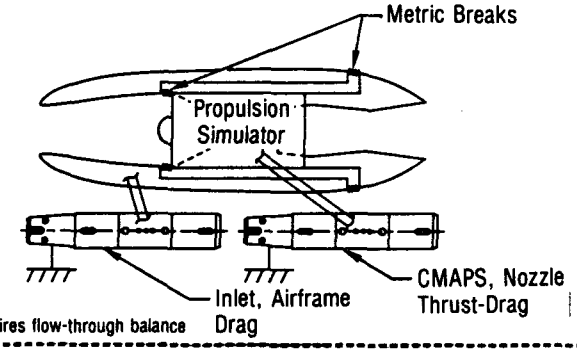

Note: Requires flow-through balance

Comments

Non-Metric:
Nothing

Metric:
Inlst, Airframe: Drag
CMAPS, Nozzle: Thrust-Drag

Calculation of:

Stream Thrust	Ram Drag
@ Plane 2	@ Plane 2
@ Nozzle Exit	

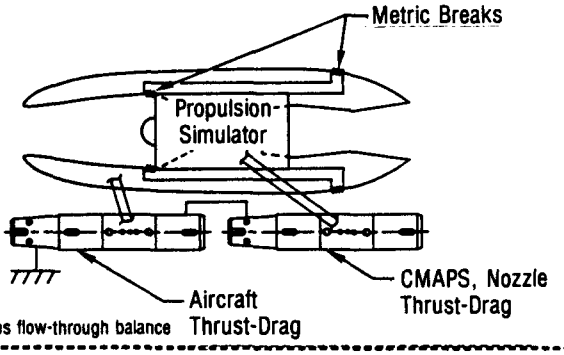

Note: Requires flow-through balance

Non-Metric:
Nothing

Metric:
Aircraft: Thrust-Drag
CMAPS, Nozzle: Thrust-Drag

Calculation of:

Stream Thrust	Ram Drag
@ Plane 2	@ Plane 2
@ Nozzle Exit	

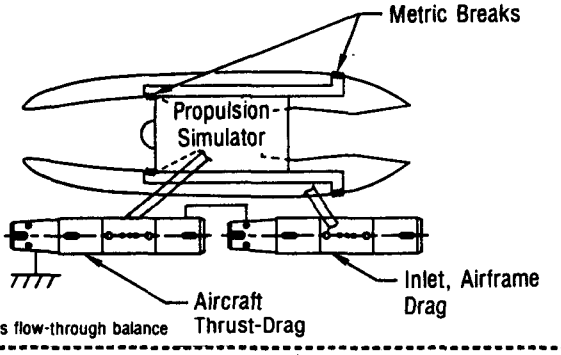

Note: Requires flow-through balance

Non-Metric:
Nothing

Metric:
Aircraft: Thrust-Drag
Inlet, Airframe: Drag

Calculation of:

Stream Thrust	Ram Drag
@ Plane 2	@ Plane 2
@ Nozzle Exit	

No Balance Concept

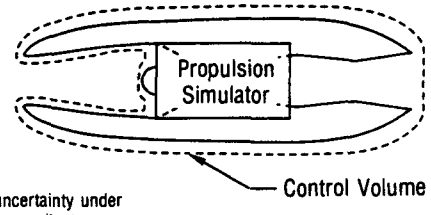

Note: Large uncertainty under pressure gradients

Comments

Non-Metric:
Full Aircraft

Metric:
Nothing

Pressure-Area Integration:
Aircraft External Surfaces, Inlet Duct to Plane 2

Calculation of:

Stream Thrust	Ram Drag
@ Plane 2	@ Plane 2

GP53-0801-29-R

Figure 5-3. (Concluded) Typical Metric Arrangements for CMAPS - Equipped Models

The metric arrangement selected for this program is considered the most straightforward concept for measuring the six aerodynamic components if thrust measurement is not a requirement. As described in Section 3, the selected arrangement consists of three metric breaks and three associated seals. The three seals are located at the simulated compressor face (duct metric break), at the beginning of the nozzle boattail (aft metric break), and between the strut and lower fuselage (strut metric break). The strut and aft metric break concepts are not new, and have been successfully employed in several recent nozzle research investigations (e.g. References 3 and 12). The duct metric break is somewhat unconventional, since usual practice for conventional flow-through testing is a completely metric internal duct. However, for a non-metric CMAPS installation, the only practical location for the duct metric break is at the CMAPS inlet.

Methods of sealing the duct metric break present a design challenge, however. This seal must provide a smooth, air-tight transition from the metric internal duct to the non-metric simulator within a relatively short distance. The Butyl rubber seal design for this model was acceptable in meeting these requirements, but could be improved. This is discussed further in Section 5.3.

A fully non-metric, pressure-instrumented model arrangement is another approach if measurement of CMAPS thrust forces are not required. However, force and moment calculations based on pressure-area integrations are subject to accuracy problems, particularly where extreme pressure gradients exist. Adequacy of such an approach obviously depends on the configurations being modeled and the Mach number/angle-of-attack combinations of interest.

5.1.3 Support System - The possible model support systems are somewhat limited. This is due primarily to the need to house two high pressure air passages (drive and bleed) for each CMAPS while maintaining the necessary stiffness in a low interference design. The primary problem is the requirement for a large passage for the turbine bleed flow. Small bleedline flow areas result in compromises to the minimum EPR line of the CMAPS flexibility map. The drive air passage is sized to deliver the desired flowrate and pressure to the CMAPS based on the available high pressure capabilities of the facility. It can therefore be smaller in size and usually has less impact on the strut size.

The bleed air lines in this strut were sized to accommodate the simulators' requirements throughout the entire flexibility envelope. This resulted in a nominal bleed line area of 9.7 sq. cm. (1.5 sq. in.) with slightly smaller areas inside the model and larger areas near the end of the support strut, as shown in Figure 5-4.

Some simulator applications may not require the capability to cover the entire flexibility map. For example, many advanced turbojet or low bypass ratio turbofan engines are expected to operate at higher average EPRs than demonstrated by current engines. CMAPS-equipped models which represent such configurations could possibly sacrifice the lower portion of the flexibility map to achieve a smaller bleed line area. However, the quantitative relationship between changes in the bleed line area and flexibility map must be defined. A study which defines this relationship could be performed in the NASA-Ames Propulsion Simulator Calibration Laboratory (PSCL).

The support system selected for this program was a compromise between two traditional concepts: the lower fuselage mounted "hockey stick" and the direct rear entry sting. In the chosen design (Figure 5-4), adequate internal volume and

stiffness was provided in the same maximum thickness (6.35 cm. (2.5 in.) near the model) that would be required for a "hockey stick" strut. Elimination of the vertical "blade" portion of a hockey stick was also achieved, acting to reduce interference at high angles-of-attack. In a direct rear entry sting, the aft-end is usually distorted. This was not acceptable for this program since accurate nozzle/airframe effects were required.

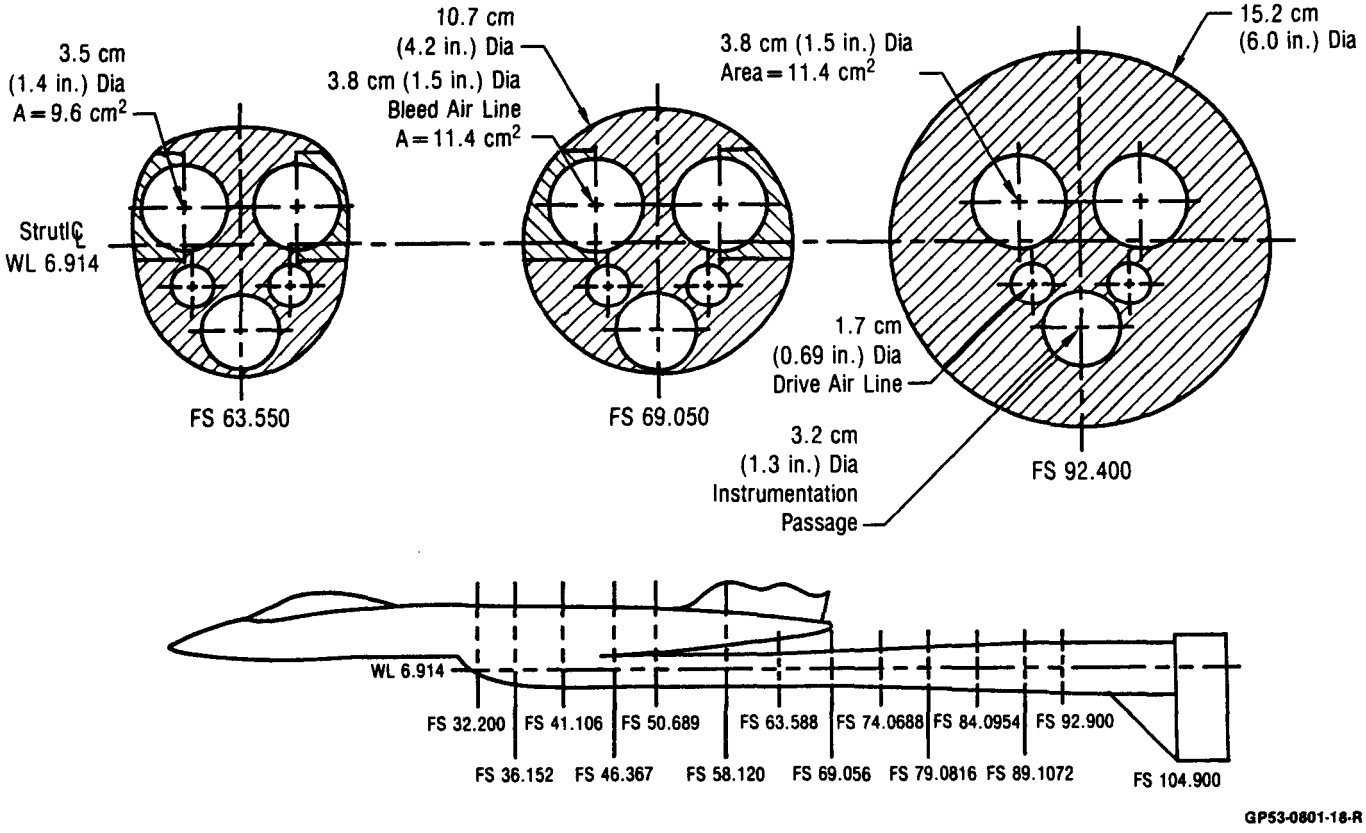

Figure 5-4. Details of Support Strut

The major disadvantage of the tested support system is the potential for increased interference at low angles-of-attack. Any interference effects should be confined to the lower aft fuselage area, which is removed from the wide-spaced inlet/nacelle/nozzle assemblies where the bulk of the interactions were identified. However, it must be assumed that any strut interference would be reflected as a common bias error among the various test modes.

5.1.4 Temperature Control - Models equipped with propulsion simulators are subject to a wider range of temperatures than conventional models. Conventional models are heated by the tunnel freestream and by any high pressure air delivered to the model. In many high speed wind tunnels, temperature gradients inside a model can generally be minimized by controlling the freestream total temperature and the nozzle air supply temperature. However, CMAPS-equipped models are subject to additional heat sources which cannot be independently controlled to minimize the temperature gradients.

The three main temperature sources from a simulator are: (1) turbine drive air at nearly 93 deg C (200 deg F), (2) turbine bleed air at 10 to 74 deg C (50 to 165 deg F), and (3) compressor discharge air up to 204 deg C (400 deg F). Significant errors may be introduced in the force and moment results if these temperature differences create a thermal gradient across the internal strain-gage balance. Therefore, an active temperature control system will normally be required to hold the balance at a pre-determined, uniform temperature.

The thermal control system for this program consisted of four separate heater blankets with feedback control. This system was designed to maintain a nominal uniform balance operating temperature of 71 deg C (160 deg F) throughout the test. A schematic of the heater/thermocouple arrangement is shown in Figure 5-5. Two heaters (#1 and #2) were located on the forward and aft sections of the balance housing. Another heater (#3) was located on the forward end of the balance taper insert. The fourth heater (#4) was located beneath the balance. Very thin (0.076 cm (0.030 in)) custom heaters, manufactured by the Watlow Corporation, were used for this application. Two of the heater blankets (#1 and #2) can be seen in the photograph of the partially assembled model is shown in Figure 5-6.

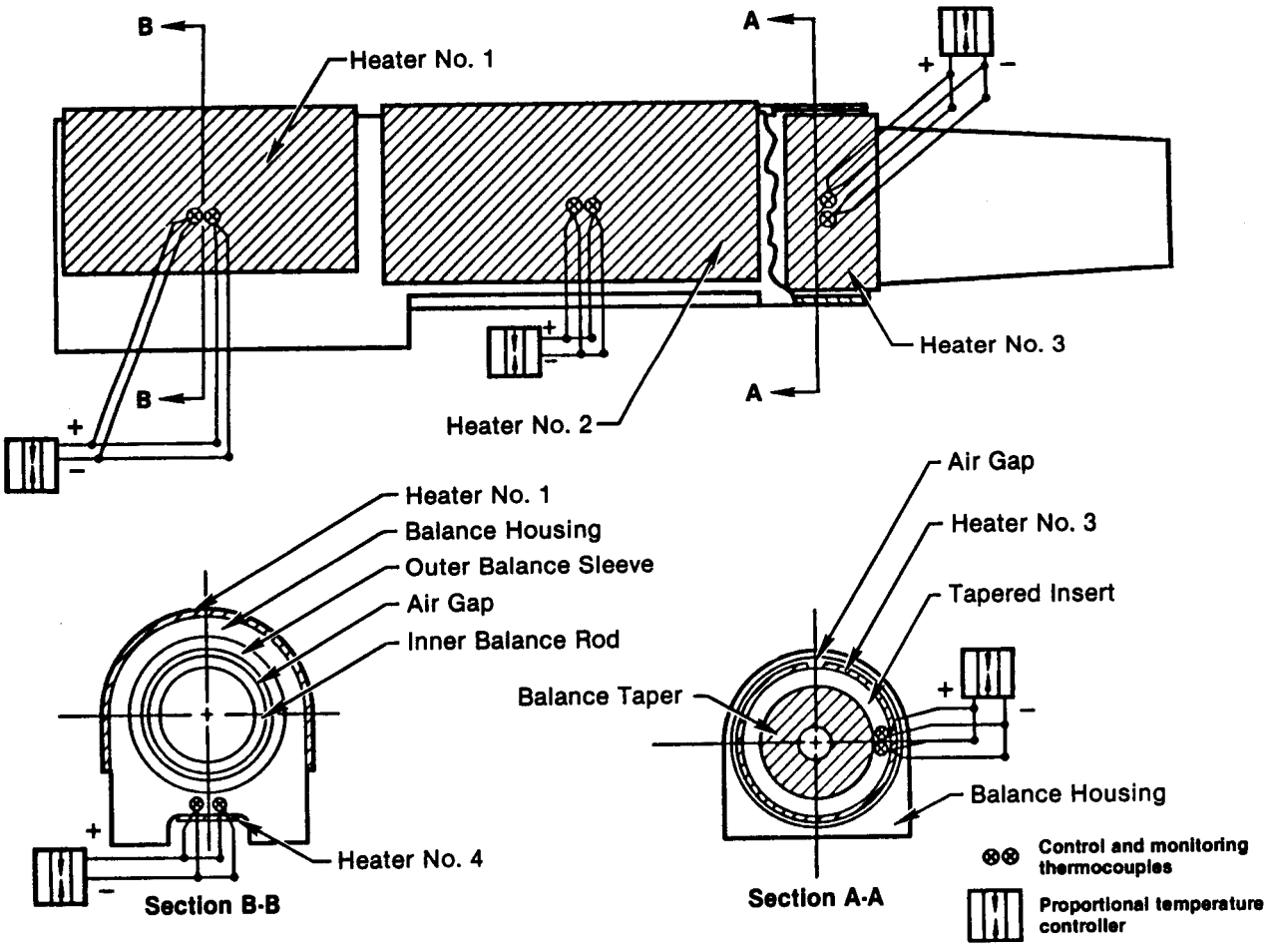

Figure 5-5. Balance Thermal Control System

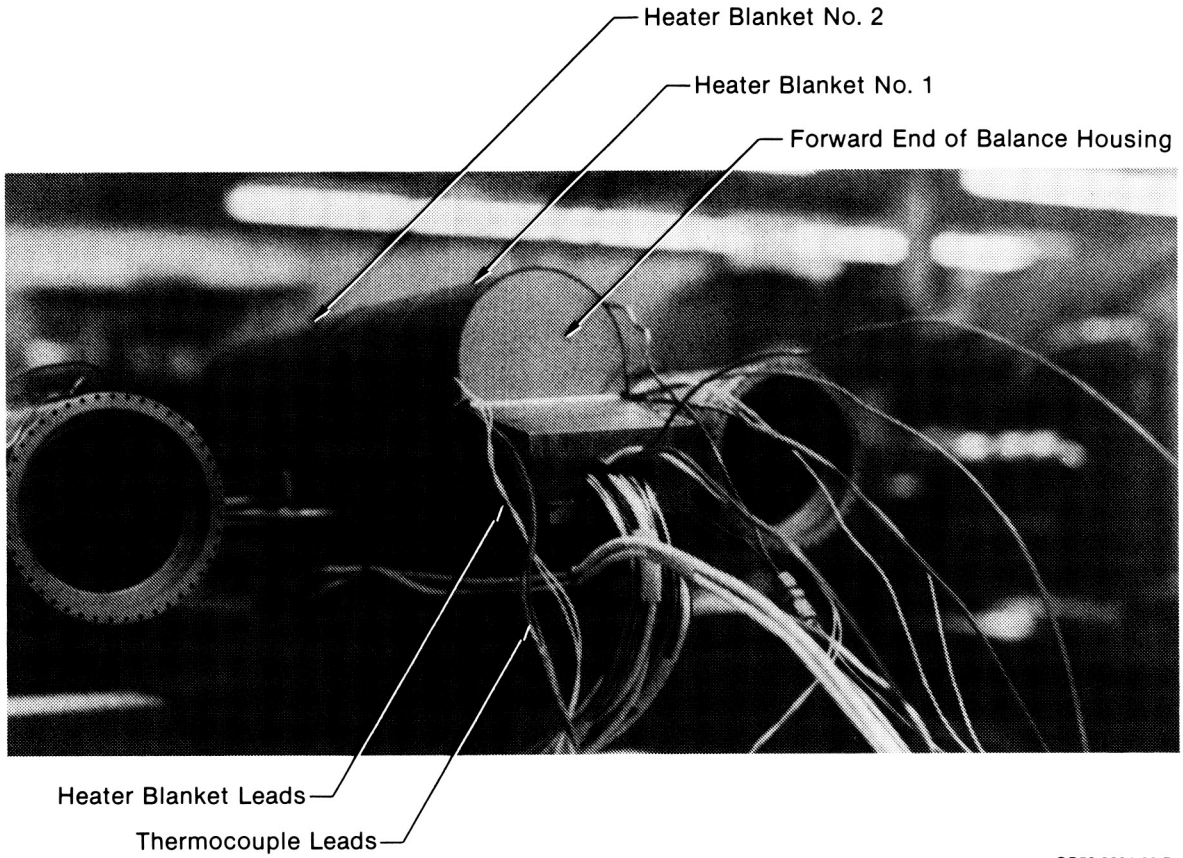

Figure 5-6. Heater Blanket Installation to Balance Housing

Two thermocouples were provided for each of the four heaters. One provided feedback to the proportional temperature controller. The other thermocouple supplied information to the data acquisition system for monitoring and back-up purposes. To avoid direct contact with the heaters, the thermocouples were installed in wells milled into the balance housing and taper adapter. The installation wells and trenches for the electrical leads for three of the thermocouples are shown in the photograph of Figure 5-7.

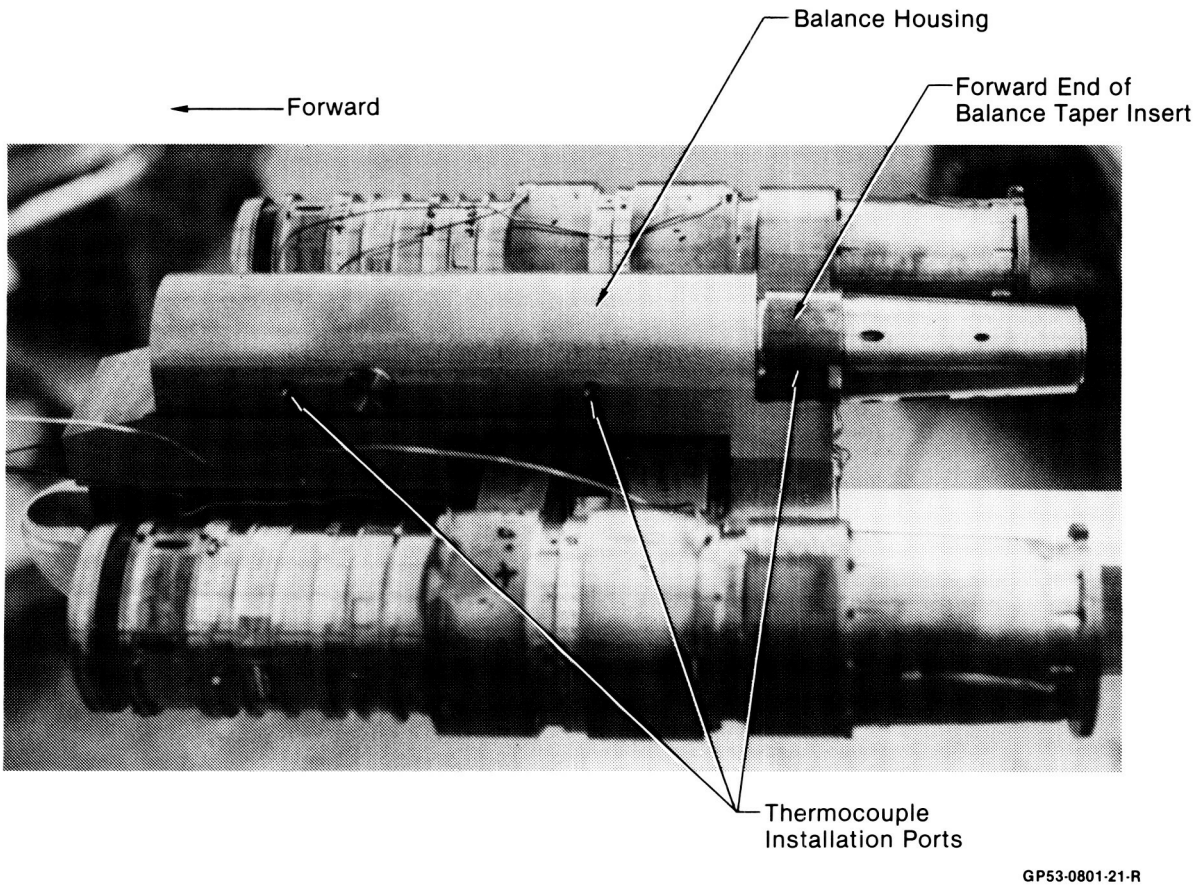

Figure 5-7. Balance Housing Prior to Heater Blanket Installation

This thermal control system maintained a nearly constant balance housing temperature despite the range and variations of temperature within the model. An example of the temperature variations at five key locations in the CMAPS and air supply system, together with variations of balance housing temperature, are shown in Figure 5-8 for an EPR sweep at Mach 0.6. Over the range of air temperatures from 22 deg C to 123 deg C (72 deg F to 254 deg F), the thermal control system maintained a nearly constant value of 71 deg C (160 deg F) along the balance housing.

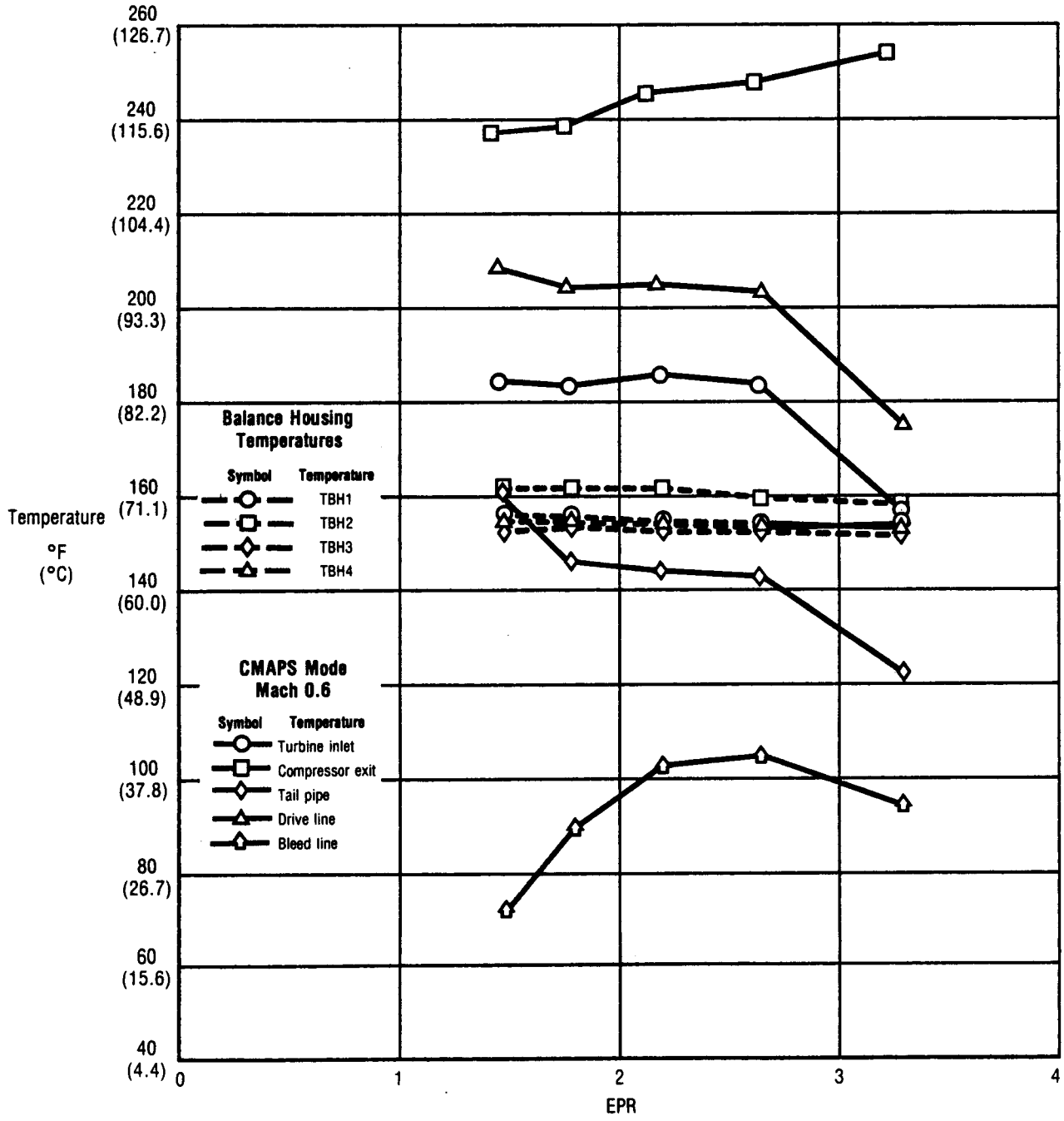

Figure 5-8. Model and Balance Housing Temperature Variation With EPR

5.2 PRE-TEST CALIBRATIONS - CMAPS-equipped models require pre-test calibrations in addition to those normally performed on a powered model. These calibrations are for inlet airflow, nozzle pressure ratio, and nozzle airflow.

5.2.1 Compressor Inlet Airflow - Similar to a full scale inlet/engine installation, compressor inlet airflow for a CMAPS cannot be accurately measured with conventional compressor face pressure instrumentation. Therefore, alternate methods of calculating inlet airflow are being developed based on pressure measurements inside or downstream of the CMAPS units. Currently, the airflow calculation methods require a separate CMAPS calibration for each mixer/nozzle combination to be tested in the wind tunnel.

In this program, both CMAPS units were calibrated statically for airflow in the NASA-Ames 9x7 ft wind tunnel. Four separate methods of calculating airflow were investigated based on measurements at the compressor face, the compressor exit, the turbine exit, and the nozzle entrance. A photograph of the simulators in the 9x7 ft wind tunnel during the static airflow calibrations is shown in Figure 5-9. The right hand CMAPS is shown with the bellmouth inlet and the ALBEN installed. The bellmouth inlet was used to provide the reference airflow. For this program, the calibrations at two different mixer/nozzle combinations required about 5 weeks. For future test programs, these calibrations would be conducted by the facility with no adverse schedule impact to the user.

Based on the NASA static calibrations, the airflow calculated from measurements made at the turbine exit was selected as the primary airflow for all of the data reduction analysis. Details of this airflow calculation method and others investigated are presented in Volume III, Reference 6.

5.2.2 Nozzle Pressure Ratio - The pressure distortion generated by a CMAPS mixer may adversely affect the measurement of average total pressure in the region immediately downstream of the simulator. In order to accurately calculate nozzle pressure ratio (NPR), therefore, the nozzle total pressure instrumentation should be calibrated prior to the test.

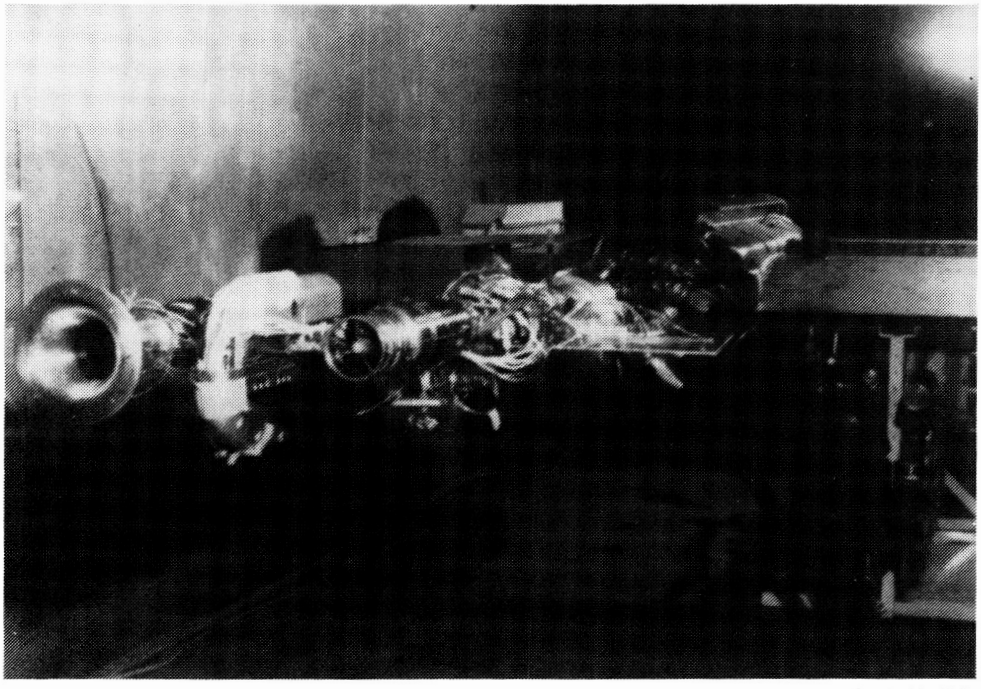

GP53-0801-10-R

Figure 5-9. CMAPS Airflow Calibration Set-Up

In this program, NASA-Ames performed the nozzle total pressure calibration during the inlet airflow calibrations. An external rake, shown in Figure 5-10, was positioned to measure total pressure at the throat of the ALBEN. The total pressures measured at the 4-probe total pressure rake located just upstream of the nozzle were then compared with those measured with the external rake, thus generating a calibration factor. The calibration arrangement is shown schematically in Figure 5-11. A drawback to this technique is the potential for adverse effects of blockage or flow angularity. In this program, the blockage effects were isolated by performing comparative runs with and without the external rake. These effects were incorporated into the calibration factors.

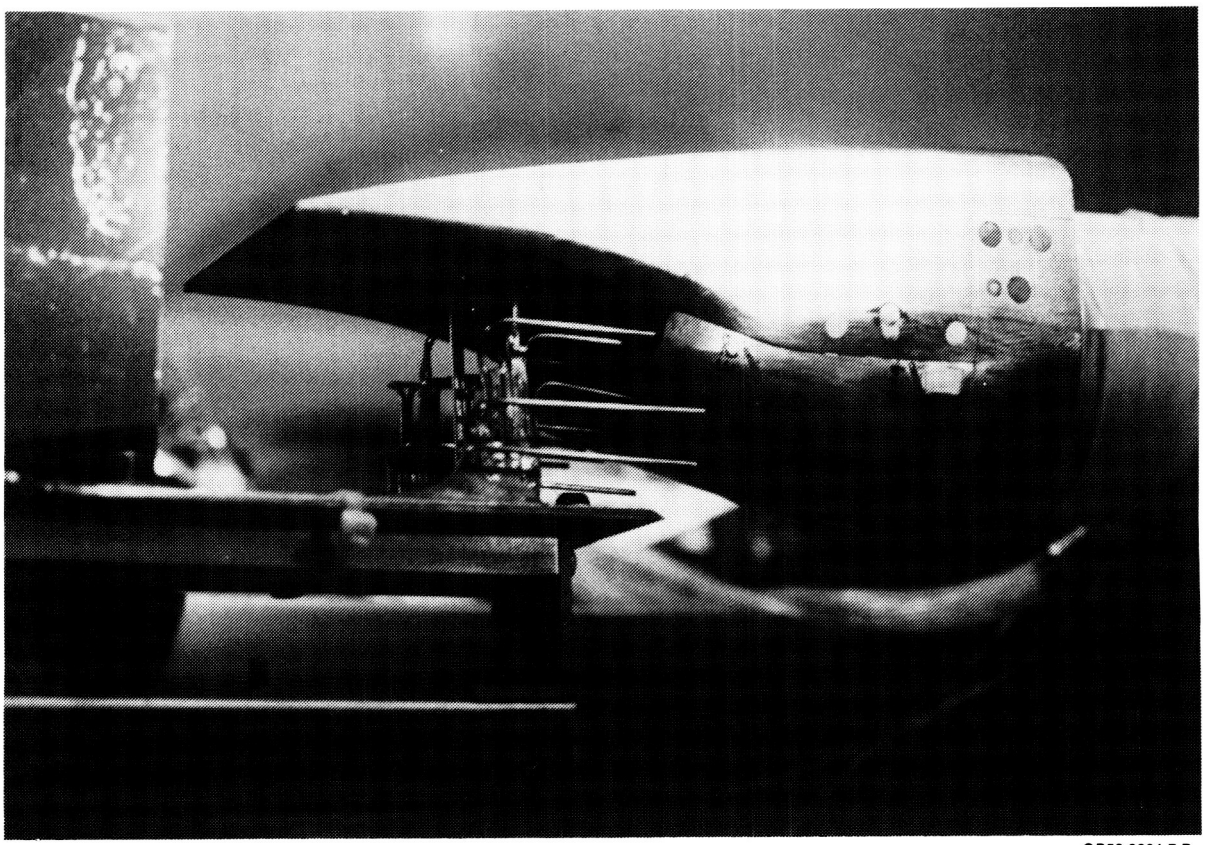

GP53-0801-7-R

Figure 5-10. External Rake for ALBEN Total Pressure Calibration
Dry Power ALBEN

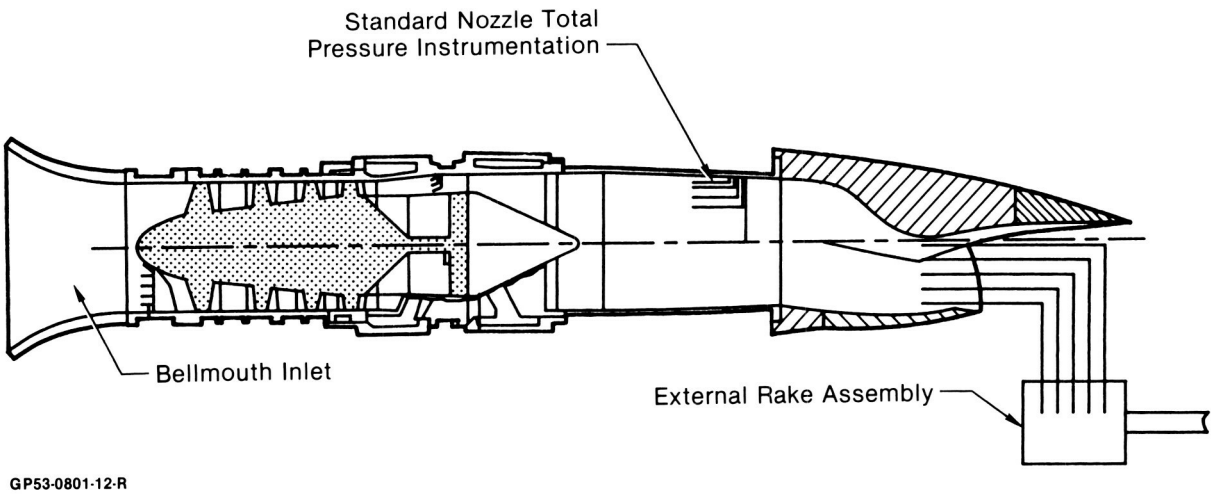

GP53-0801-12-R

Figure 5-11. Schematic of Pre-Test CMAPS/Nozzle Calibration Arrangement

A large range of total pressure calibration factors resulted from: 1) the changing pressure and temperature profiles downstream of the mixer and 2) the minimal instrumentation in that region. The pressure and temperature profiles changed throughout the engine operating map as the amounts of compressor and turbine discharge flows through the mixer were varied. Although repeatable to within $\pm$0.005, the calibration factors varied from 0.92 to 1.08 across the NPR range tested. This change in calibration factor is large and undesirable. An instrumentation rake mounted in the tailpipe may require at least 20 total pressure and temperature probes to more accurately account for these changing distortion levels. Further discussion on the typical pressure distortion downstream of the CMAPS mixer is provided in Reference 1.

Kiel probe surveys provide another method of calibrating nozzle total pressures without the adverse blockage effects. In this method, the nozzle approach duct just upstream of the throat is traversed by a small number of Kiel probes (one or two) to accurately measure this total pressure distribution with minimal blockage or disturbances. A Kiel probe differs from a standard total pressure probe in that the pitot probe is installed in the center of a venturi. Thus, the pressure indicated by the Kiel probe is insensitive to flow angularity up to 40 deg off axis. These probes are especially suited for measuring total pressure in a fluid stream where the flow direction is unknown or varies with operating condition, as may be the case behind a CMAPS mixer. An example of commercially available Kiel probes is shown in Figure 5-12. One disadvantage of the Kiel probe method is that it is more time consuming than using external rakes.

TYPE KA MINIATURE SENSING HEAD (1/16" DIA.)

Ordering Part No.	Sensing Head Description	Probe Diameter h	Probe Length (in.) a	Sensing Head Joining Compound	
				Metal Filler	Operating Temperature
KAA-6	1/16 in. Dia	1/16	6	High-Temp Alloy	1,500°F
KAA-8*	Miniature		8		
KAA-12*			12		
KAA-24			24		
KAC-6	Type "A"	1/8	6	Hi-Temp Alloy	1,500°F
KAC-8*	(See Illustration Below)		8		
KAC-12*			12		
KAC-24			24		

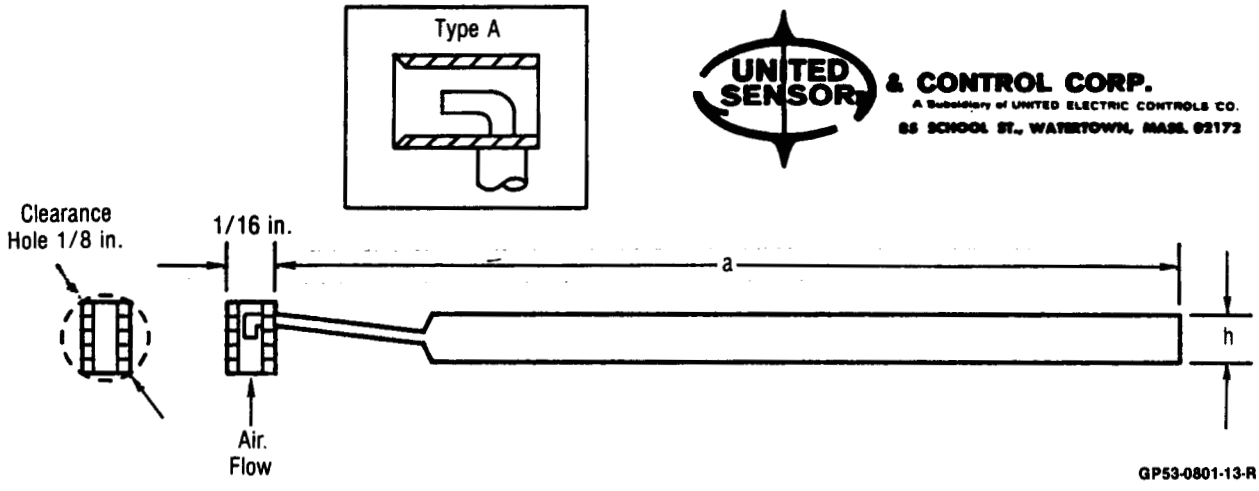

Figure 5-12. Example of Commercially Available Kiel Probes

5.2.3 Nozzle Airflow - Nozzle airflow calibrations are often conducted prior to powered model wind tunnel tests. However, standard isolated nozzle calibrations are not adequate for a nozzle to be used on a simulator powered model unless the temperature and pressure distortions typical of the CMAPS mixer are accurately simulated. Therefore, any nozzle airflow calibrations need to be performed during the other calibrations with the CMAPS. Nozzles installed behind CMAPS units can be calibrated in the NASA-Ames PSCL, where precise measurements of inlet, drive, and bleed airflow will be available.

5.3 CMAPS CONTROL AND OPERATION - The performance of the CMAPS units during the 140 hours of calibration and testing provided useful control and operation experience. The simulators proved to be reliable test tools, performing well in over 200 consecutive wind-on runs, at angles-of-attack ranging up to 20 deg and in the Mach range from 0.4 to 1.4. For these test conditions, the simulators demonstrated a significant tolerance to inlet pressure distortion.

It is not meant to imply that the CMAPS test technique is simple, or that improvements are not possible. The model is complex and the amount of support equipment is significant. However, once the model and test operations were well established, the associated data acquisition rates were found to be significantly better than the conventional test techniques.

In this section, the data acquisition rate is discussed, as well as the CMAPS distortion tolerance and specific areas which require improvement in the CMAPS technique.

5.3.1 - Data Acquisition Rate - One of the major operational advantages identified for simulator testing is the potential for an improved data acquisition rate. In this program, the conventional testing (Jet-Effects and Flow-Through) resulted in 200 wind-on runs requiring 60 hours of wind-on tunnel time and 11 working days on tunnel occupancy. Testing in the CMAPS mode resulted in 224 wind-on runs, 45 wind-on hours, and 16 tunnel occupancy days. Therefore, the CMAPS technique (at 5.0 runs/wind-on hour) acquired 50% more runs per hour than the conventional methods (at 3.3 runs/wind-on hour). During one portion of the test, the simulators were operated continuously for 8.5 wind-on hours. Continuous variations of Mach, MFR, NPR, and canard angle were performed without tunnel down time for model changes.

The improved data acquisition rate is primarily due to the operation of the CMAPS control system. The NASA CMAPS control system, Figure 5-13, is capable of monitoring health parameters and controlling the airflow and EPR of two CMAPS. In this test, the controller was placed in the AUTO RPM mode, with MFR set points obtained by "dialing-in" selected values of RPM. These set point changes took 10 to 15 seconds depending upon the size of RPM increment. The EPR set points were held manually by operating the bleed valve. The time required to change EPR set points was 40 to 50 seconds.

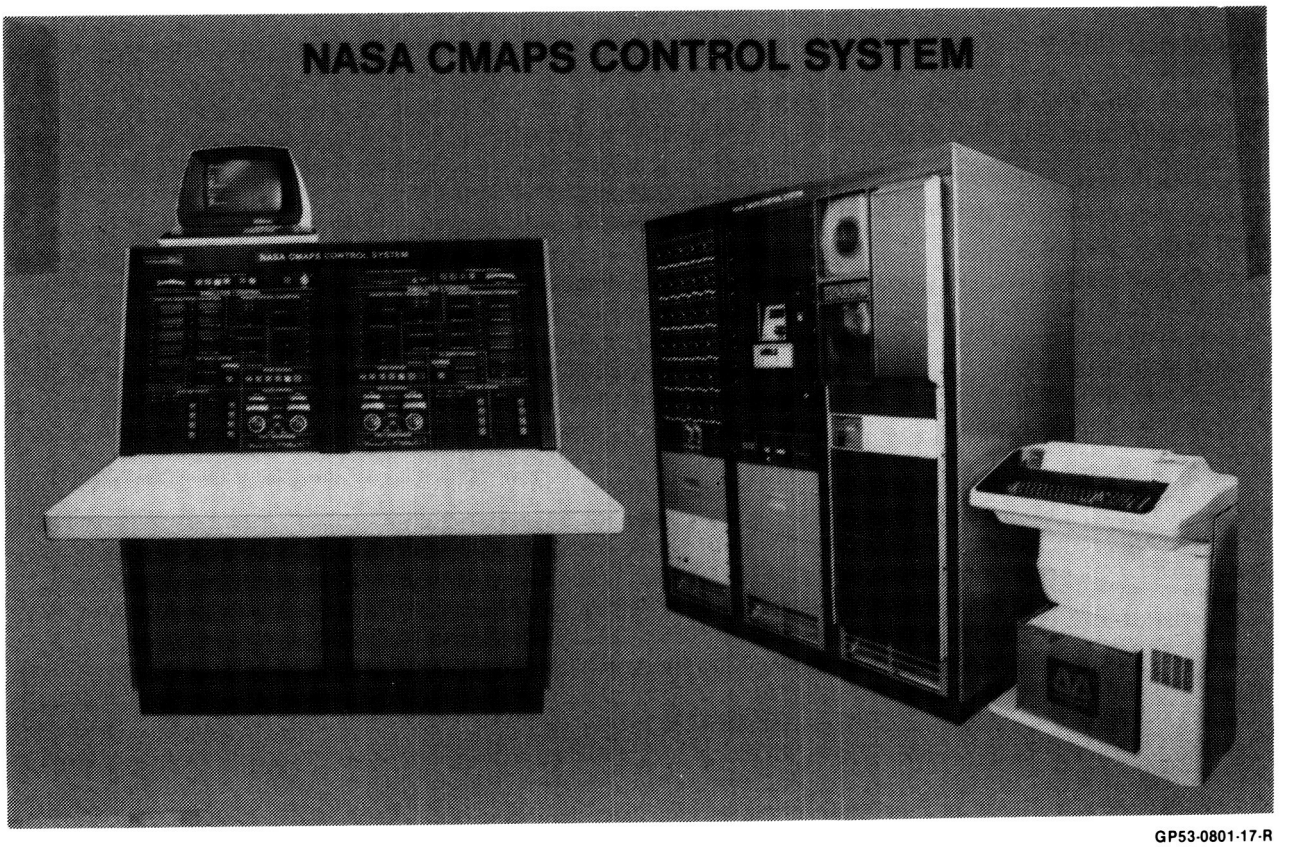

GP53-0801-17-R

Figure 5-13. NASA CMAPS Control System

The CMAPS control system is also capable of a FULL AUTO mode. In this mode, both MFR and EPR set points are dialed-in and controlled automatically. At the time of this test, an efficient algorithm for controlling inlet airflow was not available to make the FULL AUTO mode feasible.

5.3.2 Distortion Tolerance - The simulator distortion tolerance throughout the angle-of-attack and Mach ranges tested exceeded expectations. The simple normal shock inlet tested on this model produced significant levels of total pressure distortion at certain Mach and angle-of-attack combinations. However, the simulators ran problem free behind this inlet, even at distortion levels of 30% (PTmax-PTmin)/PTavg). This exceeded previously measured maximum levels of 21%, Reference 13. It should be noted however, that during high distortion conditions, the simulators were operated only at low to moderate compressor pressure ratios. 30% distortion at higher airflow conditions may have adversely affected the simulators. Also, the CMAPS controller was able to hold the RPM set points to approximately $\pm$ 1% variations at the highest levels of distortion. At distortion levels less than 15%, the controller held the set points to within $\pm$ 0.5% variations.

5.3.3 CMAPS O-ring Seals - One problem encountered in this particular test was a limitation in maximum engine pressure ratio (EPR). As the turbine inlet pressures approached 1000 psi, O-ring seals between the simulators and drive manifolds, Figure 5-14, began to leak excessively. Limits on the turbine inlet pressure resulted in a maximum EPR of 3.0, rather than the value of 4.0 that simulators are capable of attaining. A redesign of the O-ring installation should remedy this problem and permit simulators to operate over nearly the same range of inlet and nozzle conditions as current turbofan engines. NASA-Ames is currently addressing this problem.

5.3.4 Oil Supply System - Valuable experience was gained during this test regarding the type of materials used in the oil supply system of the simulator and in the model.

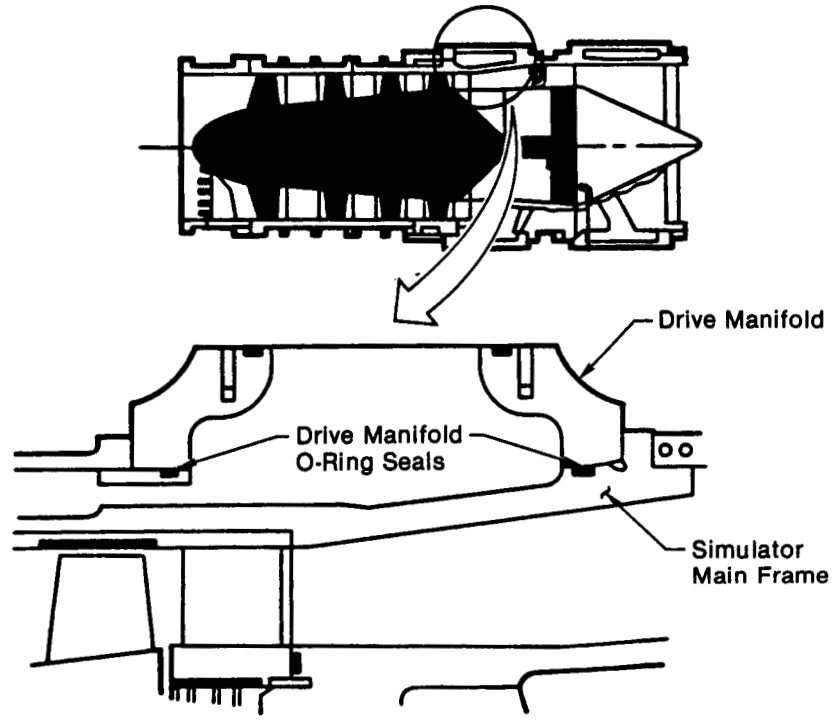

Figure 5-14. Drive-Mainfold-to-Simulator Seals

In order to allow for changes in model attitude, portions of the oil supply lines were plumbed with flexible tubing. The rate at which EPR could be increased was limited by the use of this flexible tubing. The rate at which EPR could be increased was limited by the use of this flexible tubing. This was caused by the tendency for the tubing to expand in volume as EPR increased. If EPR were increased too rapidly, the volume of the flexible tubing would also increase rapidly. However, the oil supply system could not quickly provide the oil needed to fill the extra tubing volume. This would have caused interruptions in the oil flow to the aft bearing and a sudden increase of the bearing temperature. Even slow changes in EPR would temporarily reduce the oil flow to the aft bearing, but not totally interrupt it. It was therefore necessary to place the rate in which EPR could be increased.

The use of rigid oil lines throughout the supply system is one possible corrective action, but is not always practical. Another solution might be to modify the CMAPS controller to anticipate and respond to situations which create oil deficiencies in parts of the system.

Another problem was that oil required to lubricate the simulator bearings was found to react adversely with certain types of plastic, rubber, and other petroleum-based materials used for seals and pressure tubing. Future CMAPS test programs should take steps to prevent bearing oil from pooling inside the model where it might attack these materials. One practice, which was adopted during this test, is to return the model to a nose-high inclined position during tunnel down-times. This allowed any leaking oil to drain out of the model.

Other materials with better resistance to the effects of the bearing oil might also be considered. One such material is VITON.

5.3.5 Duct Metric Break Seal - The duct metric break and associated seal (Plane 2) are peculiar to testing of non-metric CMAPS units. The seal used for this test provided a satisfactory, air-tight transition from metric to non-metric hardware. The seal created axial and normal force tares when subjected to a pressure differential or deflection. Although repeatable, these tares were not as small as desired. The duct metric break seal is therefore an area for improvement if a similar metric arrangement is used.

As the balance deflects due normal force and pitching moment loads, a vertical offset is formed between the metric and non-metric ducts. The seal must bridge the offset, as shown conceptually in Figure 5-15. The shearing stresses imposed on the duct seal during this condition create ripples in the side walls.

Further, pressure differentials across the seal cause the rubber to deform. This deformation creates an axial tare force as the tension in the seal "pulls" the metric duct aft.

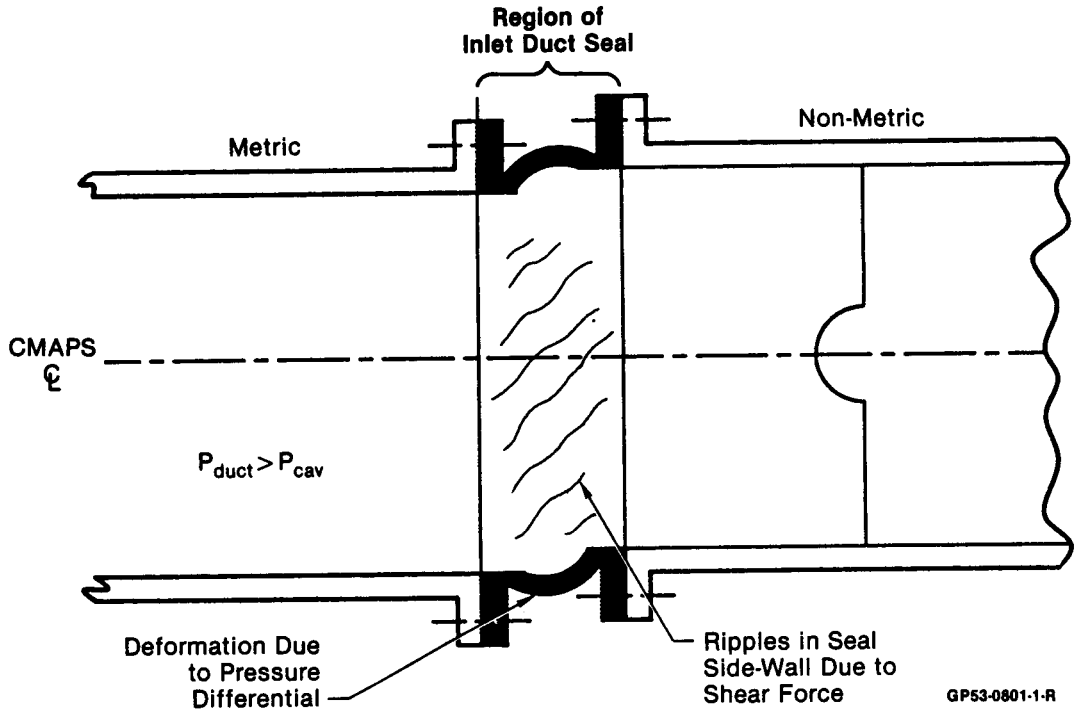

Figure 5-15. Conceptual Schematic of Duct Seal at Plane 2 Metric Break

The deformation and associated tares were alleviated in this test by installing backstops behind the seal as shown in Figure 5-16. The ripples, however, were not eliminated.

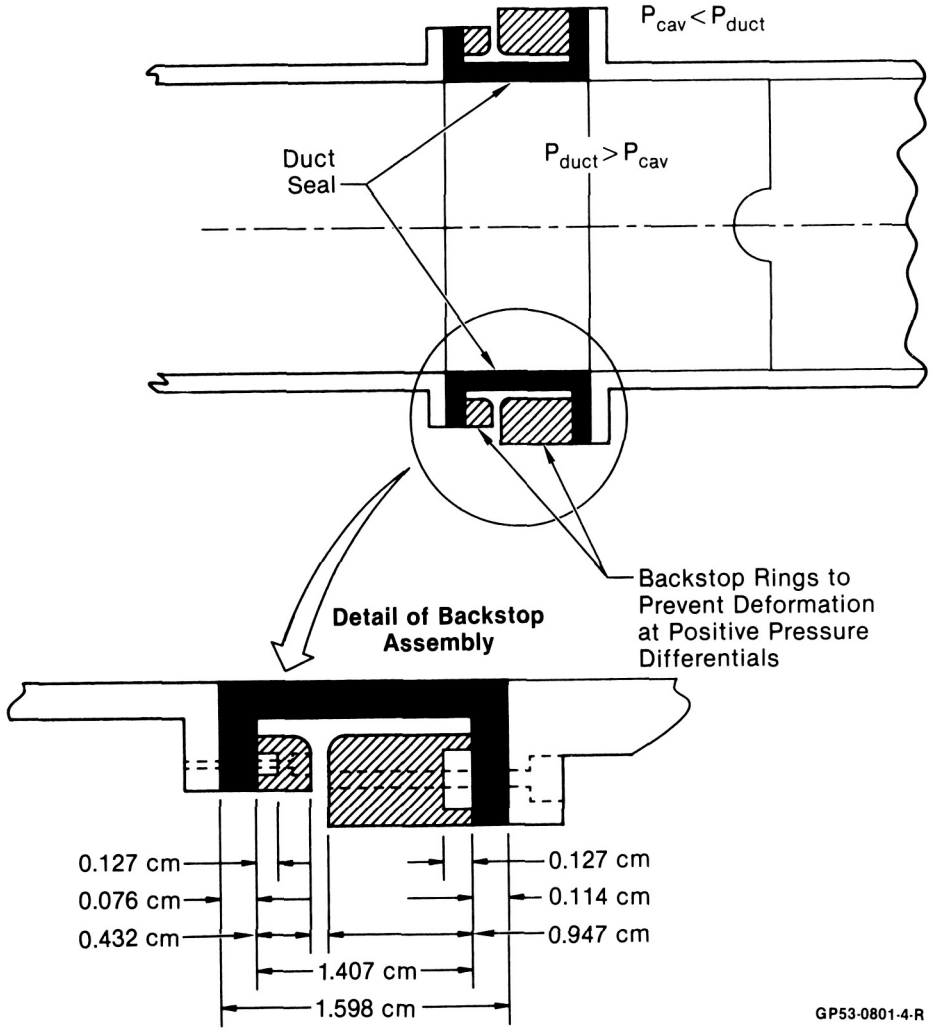

Figure 5-16. Schematic of Duct Seal With Backstop Assembly

Another method of reducing the deformation may be to fabricate the rubber seals with circumferential windings, like those used in an automobile tire. However, this approach may also be ineffective in eliminating the ripples when subjected to shear forces. An extremely short, highly flexible bellows assembly might be considered as a way to remedy both problems. However, the metal bellows designs which are currently available usually require a length of from 2 to 5 times the duct diameter to deflect into an "S" shape when placed in shear. If the "S" shape cannot be obtained, the bellows' coils will be in shear and a large normal force tare will be generated. Such a length is not feasible in most models scaled to house a CMAPS. These and other alternatives should be considered prior to future CMAPS applications.

5.3.6 Compressor Face Instrumentation Ring - The instrumentation ring at the simulated compressor face housed a 5 leg total pressure rake with a static pressure port at the base of each leg. The legs of the pressure rake, Figure 5-17, were mounted in the slots of the instrumentation ring shown in Figure 5-18. Tubing was attached to the ports on the base of each leg and routed to pressure transducers located elsewhere in the model. The ring assembly was mounted to the engine face of the CMAPS, as shown in Figure 5-19. This instrumentation ring was designed by General Electric and Tech Development Inc. for the CMAPS development program, Reference 1.

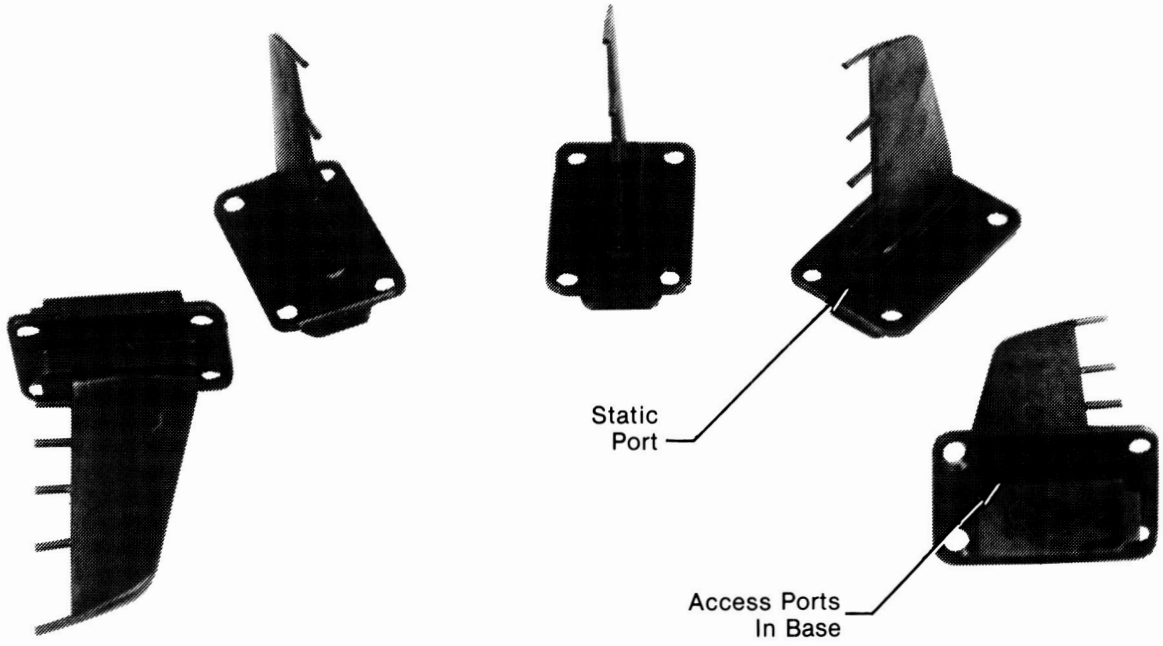

Figure 5-17. Legs of Compressor Inlet Pressure Rake

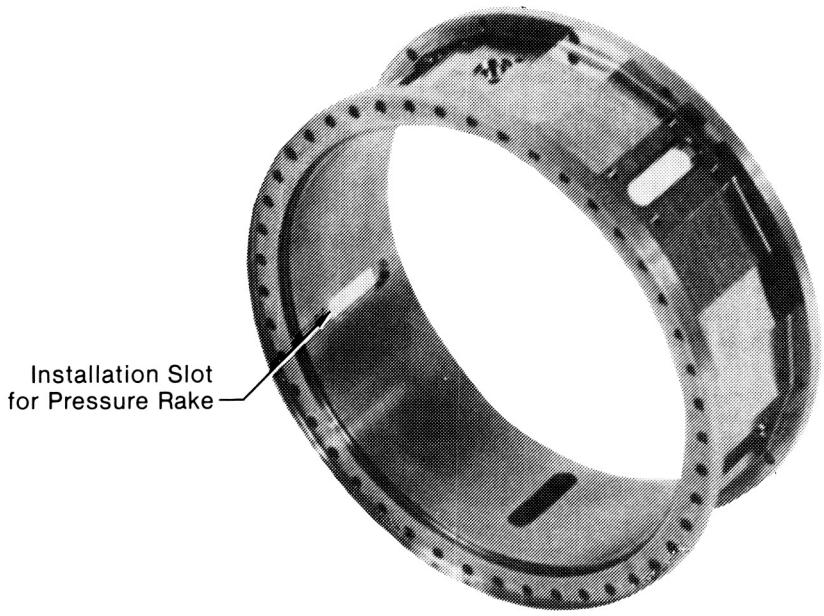

GP53-0801-6-R

Figure 5-18. Compressor Inlet Instrumentation Ring

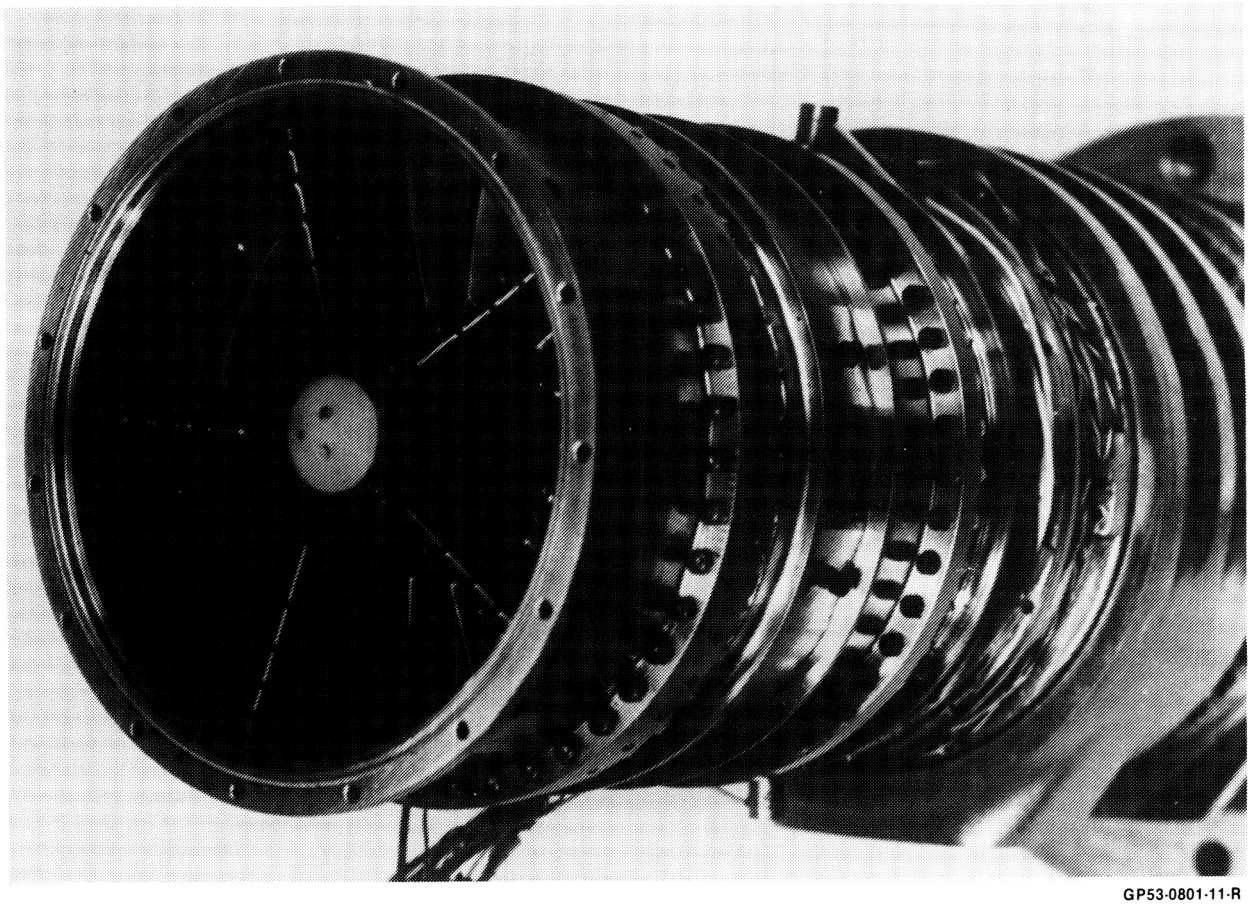

GP53-0801-11-R

Figure 5-19. Compressor Inlet Instrumentation Ring Assembly

Throughout this test, the instrumentation ring assembly occasionally experienced unacceptable pressure leaks. These leaks have been attriputed to the method of attaching the pressure tubing to the bases of the instrumentation legs. The tubing was attached with a connector block which relied on miniature O-rings for a positive pressure seal. These miniature O-rings require very precise tolerances on the mating parts to provide a positive seal If the part and the O-ring are at opposite ends of their tolerance ranges, compression of the O-ring will be decreased, and leaks are likely to occur. Furthermore, the wide range of pressure applied to these seals could cause the position of the O-rings to shift as the pressure differential changes from positive to negative. This could account for the variations in the magnitude of the leaking.

A detailed design and evaluation will be required before any changes to the instrumentation ring can be implemented. However, two possible alternate approaches to the current concept are: 1) larger O-ring assemblies and 2) stainless steel tubing routed to each pressure port on the rake and joined to flexible tubing elsewhere in the model.

5.3.7 Strut Thermal Bending - The support strut in this test experienced a thermal gradient which induced unanticipated upward bending. The thermal gradient occurred because of the temperature differences between the CMAPS drive and bleed air passing through the upper and lower portions of the strut, respectively. The airflow passages were machined directly into the structure of the strut. A simplified thermal bending analysis on the strut geometry, Figure 5-20, illustrates the problem.

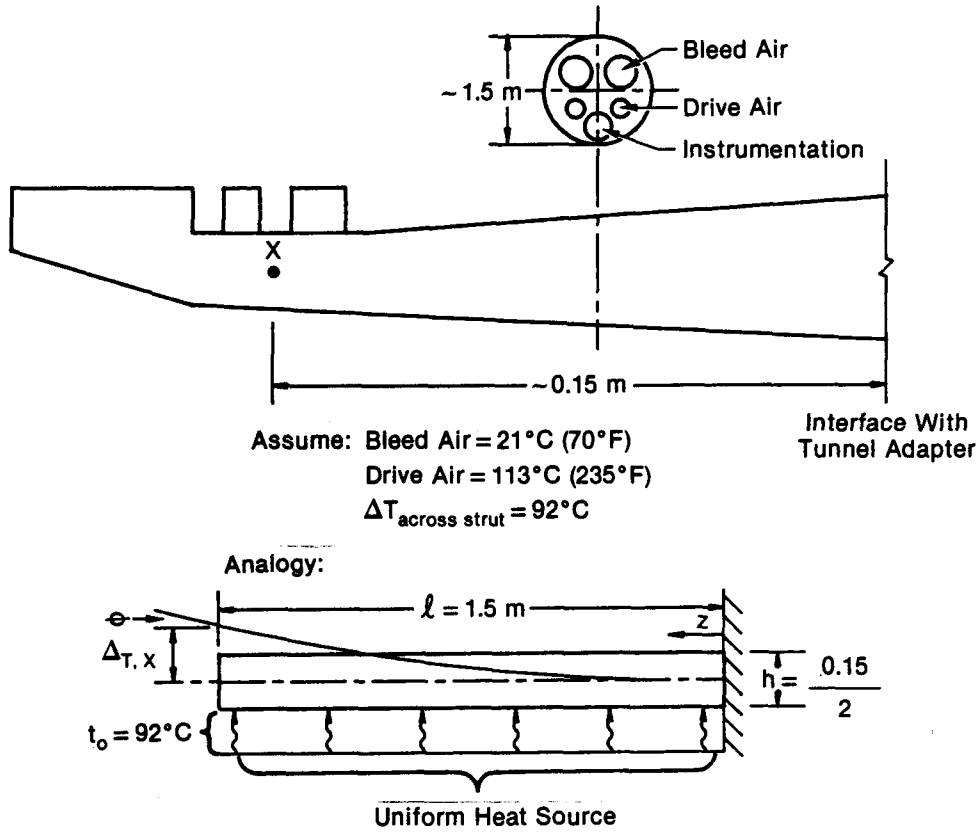

$\Delta_{T,X}$ = Deflection of Point X Due to Thermal Bending

θ = Angle of Deflected Centerline With Original Centerline

$$\Delta_{T,X} = \int_o^{\ell} z \frac{\alpha}{h} t_o \, dz$$

$$= \frac{z^2 \alpha t_o}{2h} \Big|_{z=0}^{\ell}$$

$\alpha \doteq 13.6 \times 10^{-6}$ m/m – °C

$\Delta_{T,X} = 0.0188$ m $\Rightarrow \theta \doteq 0.7°$

GP53-0801-6-R

Figure 5-20. Simplified Thermal Bending Analysis on Support Strut

In the data reduction, angle-of-attack was calculated by correcting the measured strut angle with an analytical prediction of the thermal bending, in addition to the standard corrections for elastic bending. Angle-of-attack is believed accurate to within 0.07 degrees. However, this situation could be averted in the future by designing the support system with a different drive

and bleed line arrangement. An alternate concept is shown in Figure 5-21, where the drive/bleed arrangement is designed to induce offsetting thermal gradients. Co-axial drive and bleed lines should also eliminate the gradient problem, but could be difficult and costly to implement.

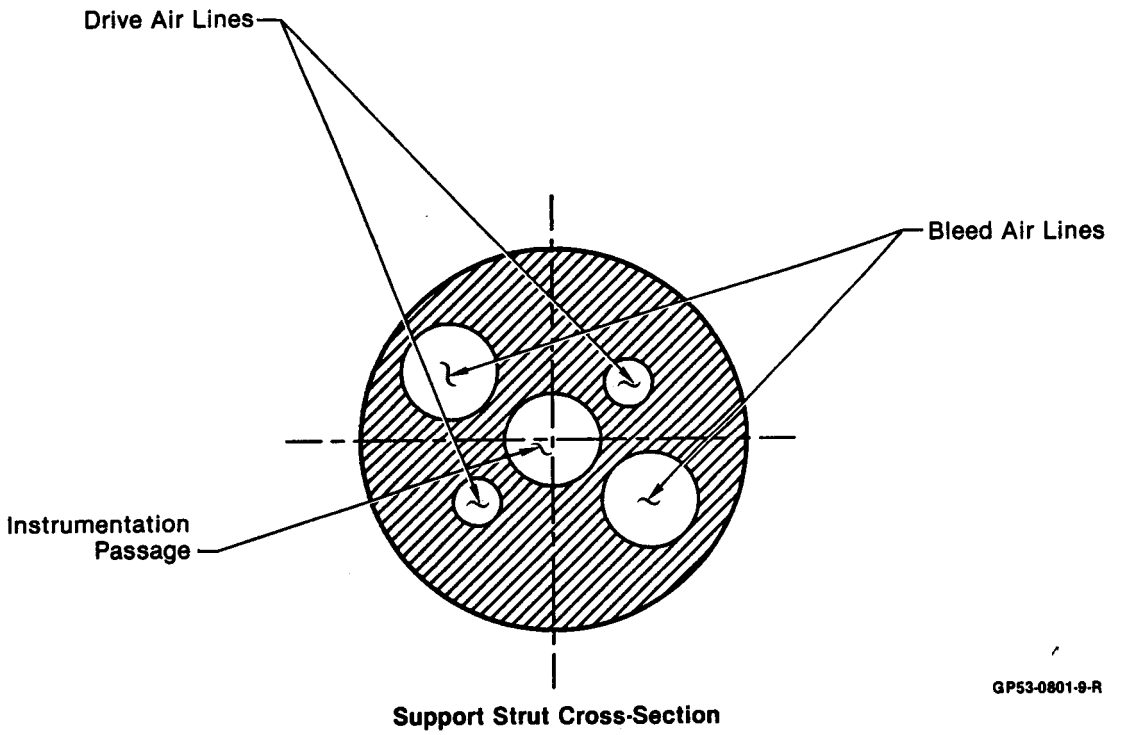

Figure 5-21. Alternate Air Line Arrangement to Avoid Thermal Bending

5.3.8 Mixer Assembly - The mixer is another area for potential improvement. The need for an improved mixer installation or variable area mixers is apparent from the simulator flexibility map (see Figure 3-5). This flexibility is defined as the range over which either compressor airflow or engine pressure ratio (EPR) may be varied while holding the other parameter fixed. EPR variations at a constant compressor airflow are achieved by directing all or part of the turbine discharge flow through the mixer to combine with the compressor flow (Figure 3-4). Variations in mixer discharge area significantly affect the obtainable EPR range for a given nozzle throat area, as discussed in Reference 2.

For each nozzle throat area tested, more than one mixer discharge area may be required to produce the desired EPR range. The model used in this program required a significant tear-down in order to change mixer assemblies. If a program involved parametrics on the nozzle throat area, such model changes could reduce or eliminate any time savings gained by using simulators. For such programs, an easily accessed mixer installation would be desirable to reduce model down time. A mixer with discrete or continuously variable discharge areas would be even more attractive.

5.4 FUTURE EFFORT - The operational experience gained in this program can be used to direct the continued development of propulsion simulators as a viable tool for wind tunnel testing. The aforementioned NASA-Ames Propulsion Simulator Calibration Laboratory can be used to address many of the developmental needs. Following this near-term development, propulsion simulators should be better suited for further wind tunnel model applications.

5.4.1 Propulsion Simulator Calibration Laboratory - The Propulsion Simulator Calibration Laboratory (PSCL) at NASA-Ames can be used to perform flowrate and thrust calibrations on any applicable hardware. The PSCL is shown in the photographs of Figure 5-22. The primary application will be the calibration of all types of turbine powered simulator (TPS) units for installed net and gross thrust under simulated ram and NPR conditions, as well as calibrations for airflow. The PSCL is scheduled for general usage in 1986 following safety qualification tests and check-out calibrations. A complete description of the capabilities of the PSCL is presented in Reference 11.

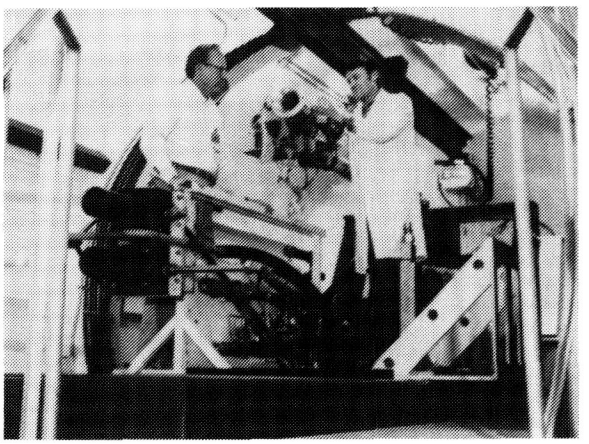

Inside PSCL Test Chamber

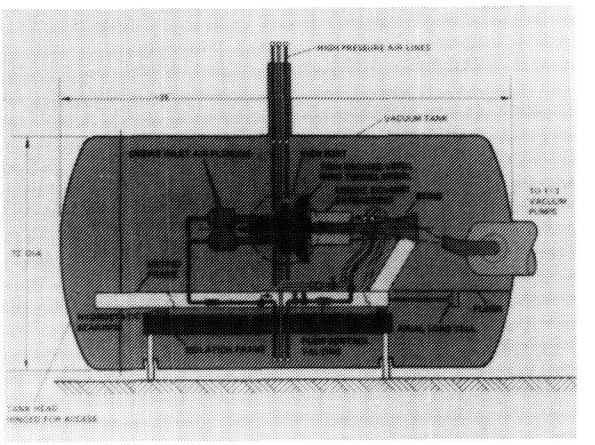

Schematic of PSCL Airflow and Balance Systems

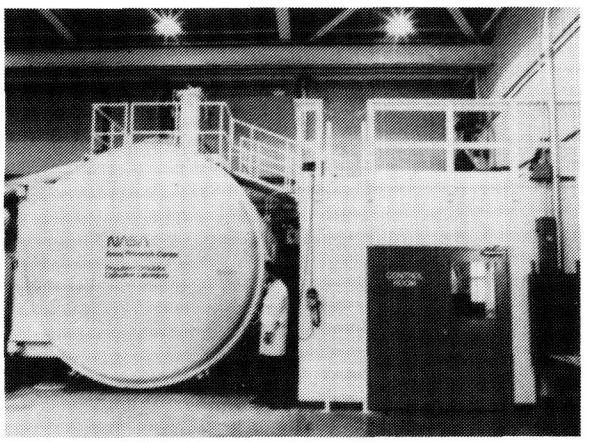

Outside PSCL Test Chamber and Control Room

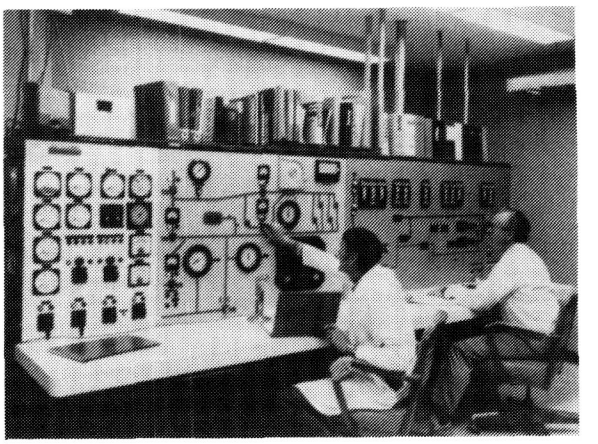

PSCL System Control Console

GP53-0801-24-R

Figure 5-22. NASA-Ames Propulsion Simulator Calibration Laboratory (PSCL)

In addition to routine calibration work, the PSCL can be used as a testbed during the development of hardware and operation improvements for the CMAPS test technique. For example, new designs for inlet duct and drive manifold O-ring seals could be fully tested and evaluated in the PSCL prior to an actual wind tunnel application. Also, the effects of pressure distortion on the CMAPS performance and airflow calculations could be more fully assessed in the controlled environment of the PSCL.

The completion of the PSCL will be a major step in the continued development of propulsion simulators.

5.4.2 Future Applications - Propulsion simulators could be of great value in the final configuration trade studies which occur in the latter stages of an aircraft concept development program. Another valuable application may be in the development of aircraft configurations which are expected to exhibit inlet/airframe/nozzle interactions. CTOL configurations which employ in-flight thrust vectoring or reversing may require wind tunnel testing with propulsion simulators in order to accurately measure the interactions. Such interactions can also be significant during the transition and hover regimes of a V/STOL aircraft. The results of this program, which was the first application of CMAPS in a full aircraft configuration, indicate that even relatively small flowfield interactions can be identified and measured when both the inlet and nozzle flows are modeled simultaneously.

The final configuration trade studies in any concept development program require an accurate definition of the propulsion system contribution to the total vehicle aerodynamic characteristics. Propulsion simulators could be used effectively in this stage of the program to measure all external aerodynamic effects related to the propulsion system (i.e., inlet and nozzle drag) on a single wind tunnel model in a single test entry. This technique would provide for the measurement of any inlet/nozzle flowfield coupling which may occur; a feature not available with the conventional combination of jet-effects and inlet drag models. These propulsion system increments could then be added to the basic vehicle aerodynamics, as measured on a conventional flow-through model, for example. Inlet performance would likely still be measured on a separate, large scale (10 to 20%) model with proper bleed and mass flow simulation and possibly variable ramp positioning. A schematic of such a CMAPS application compared to a typical conventional mode approach is shown in Figure 5-23 for a CTOL case.

Example Conventional Mode Approach

Model:

Aero Flow-Through

- Sting Mounted
- Small Scale (~5%)
- Yields Reference Force and Moment Data

Inlet Drag

- Sting Mounted
- Larger Scale (8 - 15%)
- Yields Inlet Drag at Operating MFR

Jet-Effects

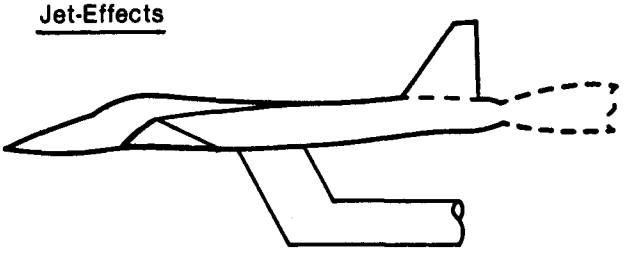

- Strut Mounted
- Inlet Faired
- Larger Scale (8 - 15%)
- Yields Nozzle Drag and Jet-Effects

Inlet Performance and Development

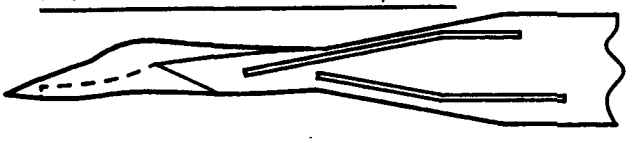

- Partial Model
- All Bleed Flows and Movable Surfaces Accurately Simulated
- Larger Scale (10 - 20%)
- Yields Inlet Internal Performance (Distortion/Recovery)

Example Simulator Mode Approach

Model:

Aero Flow-Through

- Sting Mounted
- Small Scale (~5%)
- Yields Reference Force and Moment Data

CMAPS Powered

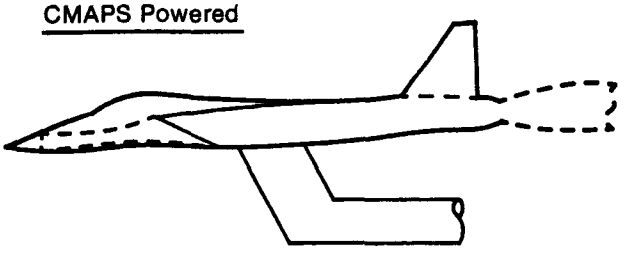

- Strut Mounted
- Larger Scale (8 - 15%)
- Inlet and Nozzle Drag Measured Simultaneously
- Interactions Measured
- Propulsion Models Reduced/Test Time Potentially Reduced

Inlet Performance and Development

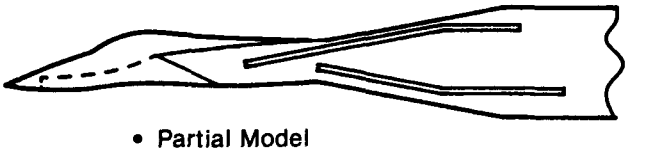

- Partial Model
- All Bleed Flows and Movable Surfaces Accurately Simulated
- Larger Scale (10 - 20%)
- Yields Inlet Internal Performance (Distortion/Recovery)

GP53-0801-28-R

Figure 5-23. Example of Aero/Propulsive Performance Testing
Conventional vs Simulator Approaches

As previously noted, V/STOL configurations may experience the most significant flowfield interaction effects, especially during the hover mode. A CMAPS-equiped model supported by an overhead support system could be used to assess these effects. The inlet and exhaust flows of the lift/cruise engines would be provided with the simulators, while either tip-driven fans or ejectors might be used to simulate the lift engines.

6. CONCLUSIONS

Supersonic propulsion simulators have been developed to provide proper simulation of inlet/airframe/nozzle flowfields on a single wind tunnel model. The effects of inlet-to-nozzle flowfield coupling were identified and measured by comparing the simulator technique to conventional Jet-Effects and Flow-Through methods. This program showed that twin CMAPS can be run in a full configuration wind tunnel model and used to identify interaction effects.

The aerodynamic coupling had the greatest impact on the supersonic drag polar, where the CMAPS mode predicted approximately 20 counts less drag (at constant lift) than the conventional mode. Subsonically, the CMAPS and conventional mode drag polars were nearly coincident, although localized interactions were identified. It is expected that configurations with vectored or dry power nozzle settings, or with closer inlet/nozzle spacing, may experience larger coupling effects.

The localized flowfield interactions were most prominent on the ALBENs, where nozzle drag in the simulator mode was as much as 10 counts different than the conventional test mode. The interactions were due to inlet MFR and canard induced effects which propagated to the nozzles.

Propulsion simulators were proven to be a generally reliable wind tunnel test tool. Potential for an improved data acquisition rate was demonstrated, provided the test sequence is tailored properly and the program schedule affords the additional pre-test activity required. The angle-of-attack range tested indicated that simulators can endure higher levels of total pressure distortion than previously anticipated. Areas for CMAPS and model design improvement were identified in several key areas, such as model scale, support system, metric arrangement, and metric break seals.

The following recommendations regarding simulator test technique are based on the experience gained from this program.

- Aircraft configurations which exhibit similar or more closely-coupled inlet/nozzle designs may require propulsion simulator wind tunnel testing to accurately predict the full configuration aerodynamic performance.

- Testing is recommended in an even closer coupled configuration to further quantify the effects of flowfield coupling.

- Propulsion simulators may be of greatest value in the latter stages of concept development, where precise results are required. For example, a CMAPS model could be used to measure all propulsion system related external aerodynamic effects (i.e., inlet and nozzle drag) in a single model. These results could be incremented to a conventional flow-through model from which the basic vehicle aerodynamic characteristics were defined.

7. REFERENCES

1. Eigenmann, M. F. and Devereaux, P. A., "Compact Multi-Mission Propulsion Simulator Development", AFWAL-TR-82-2040, September 1982.

2. Eigenmann, M. F.; Bear, R. L.; and Chandler, T. C.; "Turbine Engine Multi-Mission Propulsion Simulator Wind Tunnel Demonstration", AFAPL-TR-76-73, November 1976.

3. Hiley, P. E.; Wallace, H. W.; Booher, M. E.; and Reinsberg, J. G.; "Advanced Nozzle Concepts Program Volume III - Nozzle Integration for Air Superiority Fighter Application", AFWAL-TR-81-3165, Volume III, January 1982.

4. Zilz, D. E. and Devereaux, P. A., "Propulsion and Airframe Aerodynamic Interactions of Supersonic V/STOL Configurations - Volume I: Wind Tunnel Test Pressure Data Report", NASA CR-177343, September 1985.

5. Zilz, D. E., "Propulsion and Airframe Aerodynamic Interactions of Supersonic V/STOL Configurations - Volume II: Wind Tunnel Test Force and Moment Data Report", NASA CR-177343, September 1985.

6. Zilz, D. E.; Wallace, H. W.; and Hiley, P.E.; "Propulsion and Airframe Aerodynamic Interactions of Supersonic V/STOL Configurations - Volume III: Wind Tunnel Test Data Analysis Report", NASA CR-177343, September 1985.

7. Mraz, M. R. and Hiley, P. E., "Propulsion and Airframe Aerodynamic Interactions of Supersonic V/STOL Configurations: Phase I - Final Report", NASA CR-177369, July 1981.

8. Wagneknecht, C. D.; Dusa, D. J.; and Norbut, T. J.; "Performance Capability for a Compact Multimission Aircraft Propulsion Simulator", AIAA-83-1358, June 1983.

9. Bailey, R. O.; Smith, S. C.; and Gustie, J. B.; "Propulsion Simulation Test Technique for V/STOL Configurations", SAE-83-1427, October 1983.

10. Smith, S. C., "Determining Compressor Inlet Airflow in the Compact Multimission Aircraft Propulsion Simulators in Wind Tunnel Applications", AIAA-83-1231, June 1983.

11. M. Harper, "The Propulsion Simulator Calibration Laboratory at Ames Research Center", AIAA Paper 82-0574, March 1982.

12. Hiley, P. E.; Kitzmiller, D. E.; and Willard, C. M.; "Experimental Evaluation of Non-Axisymmetric Exhaust Nozzles", AFFDL-TR-78-185, December 1978.

13. Darlington, C. R.; Brooksbank, R. M.; and Brooks, J. O.; "Component Performance and Stability Characteristics of an Engine Propulsion Simulator with Uniform and Distorted Inlet Pressure Profiles at Reynolds Number Indices of 0.39, 0.78. and 0.91", AEDC-TR-73-172, March 1974.

1. Report No.	2. Government Accession No.	3. Recipient's Catalog No.
NASA CR-177343		

4. Title and Subtitle	5. Report Date
PROPULSION AND AIRFRAME AERODYNAMIC INTERACTIONS OF SUPERSONIC V/STOL CONFIGURATIONS VOLUME IV: FINAL REPORT - SUMMARY	Sept 85
	6. Performing Organization Code
7. Author(s)	8. Performing Organization Report No.
D. E. Zilz, H. W. Wallace and P. E. Hiley	
9. Performing Organization Name and Address	10. Work Unit No.
McDonnell Aircraft Company P.O. Box 516 St. Louis, Missouri 63166	T-3288Y
	11. Contract or Grant No.
	NAS2-10791
12. Sponsoring Agency Name and Address	13. Type of Report and Period Covered
National Aeronautics and Space Administration Washington, D.C. 20546	Contractor Report
	14. Sponsoring Agency Code
	505-43-01

15. Supplementary Notes

Point of Contact: Technical Monitor, Rodney O. Bailey
(415) 694-6265 Ames Research Center, Moffett Field, CA 94035

16. Abstract

A wind tunnel model of a supersonic V/STOL fighter configuration has been tested to measure the aerodynamic interaction effects which can result from geometrically close-coupled propulsion system/airframe components. The approach was to configure the model to represent two different test techniques. One was a conventional test technique composed of two test modes. In the Flow-Through mode, absolute configuration aerodynamics are measured, including inlet/airframe interactions. In the Jet-Effects mode, incremental nozzle/airframe interactions are measured. The other test technique is a propulsion simulator approach, where a sub-scale, externally powered engine is mounted in the model. This allows proper measurement of inlet/airframe and nozzle/airframe interactions simultaneously.

17. Key Words (Suggested by Author(s))	18. Distribution Statement
Flowfield Interactions Propulsion Simulators Supersonic V/STOL	[redacted] Until August 1987 Star Category 02

19. Security Classif. (of this report)	20. Security Classif. (of this page)	21. No. of Pages	22. Price*
Unclassified	Unclassified	73	

*For sale by the National Technical Information Service, Springfield, Virginia 22161